# TURBULENT FORCED CONVECTION OF NANOFLUID IN A HEATED TUBE: A COMPUTATIONAL FLUID DYNAMICS (CFD) STUDY

IMAN BEHROYAN

KGY110011

RESEARCH REPORT SUBMITTED IN PARTIAL FULFILLMENT OF THE REQUIREMENT FOR THE DEGREE OF MASTER OF ENGINEERING

FACULTY OF ENGINEERING

UNIVERSITY OF MALAYA

KUALA LUMPUR

2013

# UNIVERSITI MALAYA
## ORIGINAL LITERARY WORK DECLARATION

Name of Candidate: Iman Behroyan

Registration/Matric No: KGY110011

Name of Degree: Master of Mechanical Engineering
Title of Research Report:

Turbulent forced convection of nanofluid in a heated tube: A computational fluid dynamics (CFD) study

Field of Study: Heat transfer/ Nanofluid/ Computational Fluid Dynamics

I do solemnly and sincerely declare that:

(1) I am the sole author of this Work;
(2) This Work is original;
(3) Any use of any work in which copyright exists was done by way of fair dealing and for permitted purposes and any excerpt or extract from, or reference to or reproduction of any copyright work has been disclosed expressly and sufficiently and the title of the Work and its authorship have been acknowledged in this Work;
(4) I do not have any actual knowledge nor ought I reasonably to know that the making of this work constitutes an infringement of any copyright work;
(5) I hereby assign all and every rights in the copyright to this Work to the University of Malaya ("UM"), who henceforth shall be owner of the copyright in this Work and that any reproduction or use in any form or by any means whatsoever is prohibited without the written consent of UM having been first had and obtained;
(6) I am fully aware that if in the course of making this Work I have infringed any copyright whether intentionally or otherwise, I may be subject to legal action or any other action as may be determined by UM.

Candidate's Signature Date

Subscribed and solemnly declared before,

Witness's Signature Date

Name:

Abstract

In this study, turbulent forced convection of Cu-water nanofluid inside a horizontal pipe with a constant wall heat flux is investigated numerically. Two types of approaches are used; one is based on a single-phase model and the other is Eulerian-Eulerian two-phase models. The mass, momentum and energy equations are solved using control volume method (FVM) and commercial codes of ANSYS-Fluent. The simulation results of both models are compared to the existing experimental results. The simulation results for Cu-water nanofluid show that the homogeneous model, i.e., the single model is not able to predict the Nusselt number accurately for all particle fractions and Reynolds numbers. The two-phase model in Fluent can estimate the Nusselt number of nanofluid accurately, only with the use of reasonable effective particles thermal conductivities. The best effective particles conductivities are calculated based on trial and error method for some typical Reynolds numbers and particles volume fraction. Finally several correlations are developed to predict particles conductivity as a function of Reynolds number at each particle concentration. The general trend of correlations shows a linear increasing trend of the particles conductivity versus the Reynolds number.

# ABSTRAK

Dalam kajian ini, perolakan bergelora terpaksa Cu-nanofluid air di dalam paip mendatar dengan dinding malar fluks haba secara berangka. Pada pertama model dua fasa fasa tunggal dan Euleran dipilih untuk simulasi pemindahan haba. Jisim, momentum dan tenaga persamaan diselesaikan menggunakan kaedah kawalan kelantangan dan bersedia Kod komersial ANSYS-Fluent mengikut model fasa tunggal dan dua berasingan. Untuk mencari ketepatan model dalam Nusselt ramalan nombor, hasil simulasi kedua-dua model ini berbanding dengan keputusan eksperimen yang sedia ada. Pendekatan yang dipilih menunjukkan penutupan selaras dengan korelasi eksperimen berdasarkan air tulen. Para keputusan simulasi untuk Cu-air nanofluid mewakili model yang seragam tidak boleh meramalkan ukuran bilangan Nusselt tepat untuk semua pecahan zarah dan nombor Reynolds. Model dua fasa boleh menganggarkan bilangan Nusselt daripada nanofluid tepat, jika zarah berkesan kekonduksian terma diperbetulkan dengan mempertimbangkan nombor Reynolds dan kepekatan zarah betul. Jadi dengan percubaan dan kesilapan yang terbaik berkesan zarah keberaliran dikira untuk beberapa nombor Reynolds yang biasa dan zarah jumlah kecil. Akhirnya beberapa korelasi dibangunkan untuk meramalkan zarah kekonduksian sebagai fungsi nombor Reynolds pada kepekatan zarah yang berterusan. Trend umum korelasi menunjukkan peningkatan kira-kira linear dalam zarah kekonduksian dengan peningkatan dalam bilangan Reynolds. Keputusan simulasi juga menunjukkan peningkatan yang ketara dalam kekonduksian zarah sebagai zarah kecil meningkat.

# ACKNOWLEDGEMENTS

I would like to thank my supervisor, Dr. Poo Balan Ganesan at the Universiy of Malaya, who has guided my academic and professional development.I would like also to thank my parents for guiding me through my first steps of life and education. I would also like to thank my friends Ali, Hamed, Houman and Masoud for all the help and support in my study in the Malaysia.

# Contents

**List of Figures**

**List of Tables**

**Nomenclature**

**Roman symbols**

| | |
|---|---|
| A | define in Equation (4-32) |
| B | define in Equation (4-32) |
| C | correction factor |
| $C_D$ | drag coefficient |
| $c_p$ | specific heat capacity at constant pressure (J/kg.K) |
| $d_p$ | nanoparticle diameter (m) |
| $F_d$ | drag force (N) |
| h | heat transfer coefficient based on mean temperature ($w/m^2k$) |
| $h_v$ | volumetric heat transfer coefficient ($W/m^3k$) |
| $h_p$ | liquid-particle heat transfer coefficient ($W/m^2k$) |
| I | turbulent intensity |
| $I_0$ | initial turbulent intensity |
| *k* | turbulence kinetic energy ($m^2/s^2$) |
| *k* | thermal conductivity (W/m K) |
| $k_B$ | Boltzmann constant |
| $k_{pe}$ | thermal conductivity of equivalent nanoparticle (W/m K) |
| n | empirical shape factor |
| Nu | Nusselt number (h.D/k) |
| $Nu_p$ | particle Nusselt number |
| *p* | static pressure ($N/m^2$) |
| Pr | liquid Prandtl number |
| $q^{"}$ | heat flux ($w/m^2$) |
| Re | Reynolds number $(\frac{\rho v_{in} D}{\mu})$ |
| $Re_p$ | particle Reynolds number $(\frac{\varphi_l \rho_l \left\vert \vec{V}_l - \vec{V}_p \right\vert d_p}{\mu_l})$ |
| r,z | 2-D axisymmetric coordinates (m) |
| *S* | rate of deformation ($s^{-1}$) |

| | |
|---|---|
| T | temperature (K) |
| $T^{'}$ | fluctuating part of temperature (K) |
| $U^{+}$ | dimensionless velocity |
| v | velocity (m/s) |
| $V_B$ | Brownian velocity (m/s) |
| $y^{+}$ | dimensionless distance |
| $v^{'}$ | fluctuating part of velocity (m/s) |

**Greek letters**

| | |
|---|---|
| ε | dissipation rate of turbulence kinetic energy ($m^2/s^3$) |
| μ | dynamic viscosity (kg/m s) |
| $\mu_t$ | turbulent viscosity (kg/m s) |
| ρ | density ($kg/m^3$) |
| τ | shear stress (Pa) |
| $\tau^T$ | Reynolds stress (pa) |
| $\beta$ | friction coefficient($kg\ m^{-3}s^{-1}$) |
| $\kappa$ | thermal conductivity (W/m K) |
| $\Gamma$ | define in Equation (4-31) |
| $\omega$ | define in Equation (4-32) |
| ν | kinematic viscosity |
| φ | particle volume fraction |
| ψ | sphericity |
| γ | define in Equation (3-7) |
| δ | distance between nanoparticles |

**Subscriptions**

| | |
|---|---|
| cl | cluster |
| eff | effective |
| f | fluid |
| p | particle phase |
| r | radial direction |
| s | solid |

| | |
|---|---|
| w | wall |
| z | axial direction |
| - | mean |
| 0 | initial |

# 1 Introduction

## 1.1 Research Background

Since the fuel consumption has increased over the last, the heat transfer efficiency improvement has been an important research topic. So, nowadays scientists have focused on recovering heat exchanger efficiencies in different ways. The main roles of heat exchangers are absorbing the energy and then transferring it to a medium as much as possible.

Recently, scientist have found some techniques to suspend solid particles, which are powerful in conduction, among fluid molecules. At first suspending the mini and micro particles in fluids were offered. Although these particles improved the heat transfer characteristics of conventional fluids, some of problems such as high pressure drop and instability of the particles were appeared due to large size of the particles.

Approaching the particles in size of nano has solved the problem of stability and sedimentation in one hand and has increased the heat transfer efficiency on the other. Nanofluids are containing nanopowders with dimensions smaller than 100 nm and are suspended in base fluid such as water or ethylene glycol. Nanofluids were first used by Choi et al.[1], at the Argon national laboratory. Nanofluids enhance the heat transfer of the base fluids [2-4]. Because the nanoparticles are small, gravity becomes less important and thus chances of sedimentation are also less, making nanofluids more stable.

Since heat transfer mechanisms play the crucial role in the heat exchangers and cooling devices, the impact of nanofluid technology is expected to be remarkable in different industries. Almost in all industries such as transport industry or air condition system industry, reduce of size and weight are one of the important goals. Use of nanofluids can

meet these requirements by increasing the heat transfer performance. Due to the size of nanoparticles compared to microparticles the problem of clogging possibility in so narrow channels such as mini or micro-channels, is solved. In addition, the combination of microchannels and nanofluids will provide both highly conducting fluids and a large heat transfer area. Last but not least, nanofluid technology can be beneficial by pumping power reduction. In fact, for increase the heat transfer of conventional fluids by a factor of two, the pumping power must usually be increased by a factor of 10. It was shown that by multiplying the thermal conductivity by a factor of three, the heat transfer in the same apparatus was doubled [1]. Therefore by using the small fraction of nanoparticles the heat transfer enhancement can be obtained without needing to increase in pumping power.

As mentioned above, since nanoparticles have less problems of sedimentation and clogging and also enhance heat transfer of base fluid, nanoparticles suspension in fluid as a novel technique has found many capabilities in a wide range of engineering applications. In transportation application nanofluids can be associated in cooling system and increase the engine efficiency while make it lighter due to required smaller components. Moreover, since the miniaturization has been a major trend in science and technology during recent century, the microelectromechanical systems (MEMS) have been popular in industry. In this condition the conventional coolants do not have enough capability to remove the heat from high power MEMS. Thus nanofluids can be replaced in these systems without clogging impact that are common, for instance, in micro-fluids. In heating, ventilating and air-conditioning (HVAC) systems nanofluids could improve heat transfer capabilities of current industrial HVAC and refrigeration systems. Use of nanorefrigerants has been improved the heat transfer efficiency of evaporators and condensers. Consequently the nanofluid technology has made the process cycle of HVAC systems more energy efficient and cost effective.

## 1.2 Statement of the Problem

There are some theoretical and experimental works that have been done on internal flow of nanofluids under different geometries and flow regimes. Owing to increase of heat transfer by disturbing flow and also according to the popularity of turbulent flow as a common case in application, this study is focused on cylindrical tube geometry under turbulent forced convection flow. Influence of particle volume fraction on heat transfer augmentation is predicted by two different models under different high Reynolds numbers. In the single-phase model the effective thermo-physical properties are considered for simulation of forced convection heat transfer of Cu-water nanofluid whereas in the two-phase model, the nanofluid flow is considered as a two-phase flow including solid particles and base fluid. Finally the results of both models are evaluated in comparison to Xuan and Li [5] experimental results.

## 1.3 Objective of Study

The specific objectives of this research project are:

- To carry out CFD investigations of the turbulent forced convection in a heated tube using water as the working fluid.
- To carry out CFD investigations of the turbulent forced convection of nanofluids in a heated tube using a single-phase model.
- To carry out CFD investigations of the turbulent forced convection of nanofluids in a heated tube using the two-phase Eulerian-Eulerian model.
- To develop a mathematical correlation to describe the effective thermal conductivity of the nanoparticles used in the study.

## 1.4 Thesis Outline

This thesis is composed of six chapters.

**Chapter 1: Introduction.** Research background, nanofluids definition and also some applications of nanofluids in industry are described in this chapter. Finally the aims of this study and its objectives are explained.

**Chapter 2: Literature Review.** The various research investigations closely related to this study and already done including effective thermal conductivity, effective viscosity and heat transfer coefficient analysis are reviewed separately. In the last part of this chapter the literature mentioned previously, are summarized to show how the different ideas of this study were born as the objectives.

**Chapter 3: Methodology.** Since the numerical method has been adopted in this study, all steps and algorithms utilized by this work for finding the fundamental thermal data (temperature distribution) from first to end are described in this chapter. Additionally, due to the importance of single and two-phase models comparison in case of accuracy, the differentiation aspects of these two models are clarified in this chapter. Moreover the case study is explained in case of geometry and boundary conditions. Finally, according to the selected meshing type, the results of mesh dependency are illustrated.

**Chapter 4: Result and Discussion.** In this chapter first of all, the numerical approach employed in this study is validated by comparison to experimental correlations already obtained due to the literatures for water. Then the numerical predictions of each single and two-phase model applied for nanofluid simulation are assessed by existing experimental relations for cu-water nanofluid. At the end some formulas are developed for effective nanoparticles conductivity.

**Chapter 5: Conclusion.** The conclusions and contributions of this study are given in this chapter.

**Chapter 6: Recommendation for .Future Work.**

# 2 Literature review

## 2.1 History of Suspension Particle Technique

Suspension of solid particles in fluids is one of the innovative ways for improving the fluid conductivity. Various types of powders such as metallic, non-metallic and polymeric particles can be added into fluids to form slurries. It is expected that the fluids thermal conductivities are enhanced by suspension of solid particles among the fluid molecules [6]. Liu et al.[7] investigated the influences of flow rates on the pressure drop and heat transfer behavior during experimental test. Conventionally the suspended particles are employed in size of μm or even mm, although the particles in such large dimensions may cause severe problems such as abrasion and clogging. Hence, suspension of the coarse particles in fluids is not so practically applicable in industry for heat transfer augmentation.

By achieving the technique to reach the particles in nano scales, the nanofluids materials were introduced by Choi [1] for the first time. The nanofluids are some fluids involving the small measure of nano solid particles (usually between1to 100 nm) that are homogenously and stably suspended in a liquid to improve the heat transfer quality of liquids. This dispersion of solid particle makes some significant changes in thermo-physical fluid properties. In case of heat transfer views, the fluid thermal conductivity is increased remarkably as the small quantities of nanoparticles are added to fluids. Choi [1] quantitatively analyzed some potential benefits of nanofluids for augmenting heat transfer and reducing size, weight and cost of thermal apparatuses.

## 2.2 Effective Thermal Conductivity Models

A lot of models have been developed for prediction of effective thermal conductivity since the model that is offered by Maxwell [8] for spherical particles at the first time. Among the all models, roughly most of them can be categorized in two general groups

which are static and dynamic models. The former suppose the stationary nanoparticles in the base fluid and the thermal conductivity is calculated based on Maxwell correlation or its improvement whereas the latter are based on considering the random motion of nanoparticle known as Brownian motion. In this way the particle motion is considered to be in charge of heat transfer enhancement.

The classical static models such as those recommended by Maxwell[8] ,Hamilton–Crosser[9], and Wasp (Xuan and Li)[10] took into account the effective thermal conductivity of nanofluids based on a static continuum fluid in which the well-dispersed nano solid particles have been suspended . The Maxwell [8] model was offered to calculate the effective thermal conductivity of liquids with low volumetric and spherical suspended solid particles.

$$k_{eff} = \frac{k_p + 2k_f + 2(k_p - k_f)\phi}{k_p + 2k_f - (k_p - k_f)\phi} k_f \qquad \textbf{2-1}$$

Where $k_{eff}$, $k_p$, and $k_f$ are the thermal conductivity of the nanofluid, nanoparticles and base fluid, respectively. $\phi$ is the volume fraction of particles in the mixture.

This model is applicable to statistically homogeneous and low volume fraction liquid–solid suspensions with randomly dispersed and uniformly sized spherical particles.

The Maxwell model was modified by Hamilton and Crosser [9]to consider the effect of particles shape on thermal conductivity.

$$k_{eff} = [\frac{k_p + (n-1)k_f - (n-1)(k_f - k_p)\phi}{k_p + (n-1)k_f + (k_f - k_p)\phi}].k_p \qquad \textbf{2-2}$$

Where n is the empirical shape factor given by:

$$n = \frac{3}{\psi},$$

where ψ is the particle sphericity defined as the ratio of the surface area of a sphere (with the same volume as the given particle) to the surface area of the particle. Based on experimental research, there is acceptable coincidence between the theoretical results and the experimental data captured for special particles in the range of volume fractions about 30%. As the size of particles is very small (~ 100 nm) in one hand and a so fine particle can be assumed as a sphere on the other, one can conclude the sphericity of nanoparticles equal to 3.For spherical particles, the Hamilton and Crosser (HC) [9]model simplifies to the Maxwell model.

These classical models are found to be unreliable in thermal conductivity prediction because of neglecting the effects of particle size, interfacial layer at the particle /liquid interface and Brownian motion of nanofluids [11-16].

Koo and Kleinstreuer [17] considered the thermal conductivity of nanofluids to be composed of two parts:

$$k_{eff} = k_{static} + k_{Brownian} \qquad \textbf{2-3}$$

where $k_{static}$ represents the thermal conductivity enhancement due to the higher thermal conductivity of the nanoparticles and $k_{Brownian}$ takes the effect of Brownian motion into account. For the static part, classical Maxwell [8] model was proposed while for $k_{Brownian}$ Brownian motion of particles was considered. As a result, the following expression was proposed:

$$k_{Brownian} = 5\times10^{4}\,\beta\phi\rho_f c_{p,f}\sqrt{\frac{k_B T}{\rho_p d_p}}\,f \qquad \textbf{2-4}$$

where $\rho_f$ and $k_B$ are the density of base fluid and Boltzmann constant, respectively, and T the temperature in k. $C_{p,f}$ is specific heat capacity of base fluid. In the analysis, the interactions between nanoparticles and fluid volumes moving around them were not considered and an additional term, β, was introduced in order to take that effect into

account. Koo and Kleinstreuer[17] indicated that this term becomes more effective with increasing volume fraction. Another parameter, f, was introduced to the model in order to increase the temperature dependency of the model. Both f and b were determined by utilizing available experimental data.

Some researchers recommended the static models of thermal conductivity [17, 34, 35,38,40,60, 61, and 65, 67–70] employed the concept of a liquid/solid interfacial layer to justify models and to explain the conductivity increase of nanofluids. Except for Leong et al.[18] model, most of these models were developed by directly modifying the Maxwell and Hamilton–Crosser models, through the particle volume fraction. For example Yu and Choi [19, 20] developed their models by considering and applying the effect of the interfacial layer based on the Maxwell and Hamilton–Crosser models. In fact, in this regard the thermal conductivity and volume fraction of nanoparticles were replaced by the equivalent properties of particle and its surrounded nanolayer. In these models unlike the reality the thermal conductivity of nanolayer is considered the same nanoparticle. Actually the molecules in interfacial layer formed over the particles have less concentration than the solid molecules. Consequently the measure of interfacial layer conductivity is between the conductivity of solid particle and the base liquid, which is less than that of solid particle and more than that of bulk liquid. The result was substituted into the Maxwell model and the following expression was obtained.

$$k_{eff} = \frac{k_{pe} + 2k_f + 2(k_{pe} - k_f)(1+\beta)^3\phi}{k_{pe} + 2k_f - (k_{pe} - k_f)(1+\beta)^3\phi} k_f \qquad \textbf{2-5}$$

where $k_{pe}$ is the thermal conductivity of the equivalent nanoparticle;

$$k_{pe} = \frac{[2(1-\gamma) + (1+\beta)^3(1+2\gamma)]\gamma}{-(1-\gamma) + (1+\beta)^3(1+2\gamma)} k_p, \qquad \textbf{2-6}$$

where

$$\gamma = \frac{k_l}{k_p}, \qquad \textbf{2-7}$$

and $k_l$ is thermal conductivity of the nanolayer. $\beta$ is defined as:

$$\beta = \frac{t}{r_p}, \qquad \textbf{2-8}$$

where t is nanolayer thickness and $r_p$ the nanoparticle radius.

. Jang and Choi [12, 15] considered the effect of Brownian motion of nanoparticles in their thermal conductivity model of nanofluids. Accordingly, the proposed model is a function of both fluid and particle conductivities, temperature and size of particles. In addition they explained the reason of heat transfer enhancement due to four mechanisms including heat conduction in both base fluid and nanoparticles, collisions between nanoparticles (according Brownian motion), and micro-convection caused by the random motion of the nanoparticles. Among these, the collisions between nanoparticles were found to be negligible when compared to other modes. Theoretically the Brownian motion is created by the random bombardment of liquid molecules. Then the particles move through the liquid randomly. Then the heat transfer mechanism is strengthened rather than when there is only conduction mechanism. So this means an increase in the effective thermal conductivity. It should be considered that Brownian motion would be important mechanism, if it is more dominant than diffusion in the fluid.

Keblinski et al. [12] explained four possible mechanisms for the enhancement of nanofluids heat transfer including: (i) Brownian motion of the nanoparticles, (ii) liquid layering at the liquid/particle interface, (iii) nature of the heat transport in the nanoparticles, and (iv) the effect of nanoparticle clustering. On the other hand, by a simple analysis, Keblinski et al.[12] showed that the thermal diffusion is much faster than Brownian diffusion, even within the limits of extremely small particles.

Since nanoparticles are able to form clusters according Prasher et al. and; He et al[21, 22], Evans et al. [23] suggested that clustering can cause higher speed transport of heat along the large distances in comparison to heat transfer by liquid molecular structure. The thermal conductivity dependencies of nanofluids on clustering and interfacial thermal resistance were studied in this work. Effect of clusters was assessed in three steps by using Bruggeman model [21, 24], the model by Nan et al. [25] and Maxwell–Garnett (M–G) model based on Prasher et al. [21] and Wang et al.[26] studies. Finally the thermal conductivity ratio expression was resulted as:

$$\frac{k_{eff}}{k_f} = \frac{(k_{cl} + 2k_f) + 2\phi_{cl}(k_{cl} - k_f)}{(k_{cl} + 2k_f) - \phi_{cl}(k_{cl} - k_f)} \quad \textbf{2-9}$$

where $k_{cl}$ is the thermal conductivity of the cluster and $\phi_{cl}$ is the particle volume fraction of the clusters, which are defined in the study and the related expressions are also given to calculate effective thermal conductivity theoretically [26]. Although clustering at a certain level may augment thermal conductivity, extreme clustering can result in a negative consequence because of sedimentation [21].

In nanofluid flows the temperature changes can play a crucial role to influence the thermal conductivity. In fact the temperature variances impact on the Brownian motion and clustering of nanoparticles. This leads to significant changes nanofluids thermal conductivity [27]. Furthermore, some researchers have claimed that the use of temperature-dependent properties of nanofluid, especially temperature-dependent model of thermal conductivity, in computational studies can result in more precise results [28]. The temperature-dependent conductivity and viscosity based on experimental correlations of Putra et al. [29] were employed by Palm et al.[28] and Namburu et al.[30]. Finally, it was concluded that accounting temperature in relations for nanofluids properties led to more accurate prediction of heat transfer performance.

## 2.3 Effective Viscosity

Viscosity as one of the inherent properties of a fluid effects on heat transfer phenomena significantly. After adding the nanoparticles to fluid, depending on the particles volume fraction, temperature and methods of particle suspension, the Newtonian or non-Newtonian behaviors are appeared by the fluid [31-34].

The effective viscosity of nanofluids is claimed to be sensitive to temperature and particles concentration according to several studies [11, 31, 33, 35-37]. The effective viscosity increases by increasing particles concentration while it decreases with increase in temperature.

The effective viscosity equation was developed by Einstein [38] for a dilute suspension of small particles:

$$\mu_{nf} = (1 + 2.5\phi)\mu_f \qquad \textbf{2-10}$$

where $\mu_f$ and $\phi$ are fluid viscosity and nanoparticle volume fraction respectively.

Then for suspension of finite concentration Mooney [37] extended Einstein equation. Later a general form equation was offered by Brinkman [39] obtained by modification of the Einstein equation[38]:

$$\mu_{nf} = \frac{\mu_f}{(1-\phi)^{2.5}} \qquad \textbf{2-11}$$

The experimentally measured nanofluids viscosities deviate from the classical model because these models consider viscosity as a function of volume concentration only and there is no consideration of temperature dependence [32].

The viscosities of the dispersed fluids with $\gamma$-$Al_2O_3$ and $TiO_2$ particles were measured by Pak and Cho at a 10% volume fraction of particles. The results showed roughly a three

times higher viscosity than that of water [40]. According to Wang et al [11] study 20 to 30% increase in viscosity of water was observed when 3% volume fraction of $Al_2O_3$ nanoparticles was added to water. Das et al.[19] showed the increase of viscosity with particles volume fraction. In addition to this, they found that after particles addition the fluid keeps its typical Newtonian nature. Similarly, Namburu et al.[30].found that ethylene glycol and water mixture loaded by nano $Sio_2$ particles show the non-Newtonian behavior at temperature below -10$^o$C whereas Newtonian properties are appeared at above -10$^o$C.

Chen et al. [41] categorized the rheological behavior of nanofluids into four groups as dilute nanofluids, semi-dilute nanofluids, semi-concentrated nanofluids, concentrated nanofluids.

Xinfang et al.[42] measured the viscosity of cu-water nanofluid by using capillary viscometers. They found that the temperature is the main factor influencing the viscosity of the cu-water nanofluid.

Recently the new model of effective viscosity by considering the Brownian motion was offered by Masoumi et al. [43]:

$$\mu_{nf} = \mu_f + \frac{\rho_p V_B d_p^2}{72C\delta} \quad \textbf{2-12}$$

where $V_B$ , $\delta$ and C are Brownian velocity, distance between the nanoparticles and correction factor respectively. In addition $V_B$ and $\delta$ are defined as follows:

$$V_B = \frac{1}{d_p}\sqrt{\frac{18k_B T}{\pi\rho_p d_p}} \quad \textbf{2-13}$$

$$\delta = \sqrt[3]{\frac{\pi}{6\phi}}d_p \quad \textbf{2-14}$$

And also $k_B$ represents Boltzmann constant.

The nanofluid viscosity is predicted by this model as a function of temperature, mean particle diameter, particle volume fraction, density of particle and the base fluid physical properties.

### 2.4 Heat Transfer Analysis

In case of nanofluids, there are many experimental investigations. K.B.Anoop et al. [44, 45] carried out experiments to analyze the effect of nanoparticles on heat transfer coefficient. In this study alumina nanoparticles, in sizes 45 nm and 150 nm, and water as a base fluid were used in fully developed laminar regime. The results showed the augment of heat transfer as a result of nano-solid particles among water. In addition, the nanoparticles having smaller sizes cause more improvement in heat transfer efficiency. Wen and et al [46] carried out an experiment about the heat transfer of $Al_2O_3$-water nanofluid in the entrance region of a uniformly heated-wall tube. Their results showed a remarkable increase in heat transfer efficiency especially in the entrance region of the tube. They justified the phenomena because of the particle migration effect (inhomogeneous nanoparticle volume fraction) that declines the thickness of thermal boundary layer. Heris et al. [47] studied CuO-water and alumina-water nanofluids in an annular tube. Based on the comparison between the experimental results and single-phase model results they reported that the homogeneous single-phase model under-predicts the heat transfer augmentation, especially in higher particle volume fraction. Xuan and Li [5, 48] did experiment to study the heat transfer coefficient of Cu-water nanofluid of 0.3 to 2% volume fraction. According to the results, Nusselt number of Cu-water nanofluid is enhanced up to 60% with only 2% volume concentration. Yang et al. [49] presented the experimental investigation on convective heat transfer of graphite-water nanofluid in a horizontal pipe. The influence of Reynolds number, volume concentration and temperature on heat transfer coefficient has been assessed during the study. Finally as the results illustrated heat transfer coefficient increases with the Reynolds number and

particle concentration. Experimental analysis of oxide nanofluid has been done by S.Zeinali et al. [47] throughout a constant wall temperature pipe and laminar flow regime. CuO and $Al_2O_3$ water nanofluids were used in this experiment. First of all the results indicated the heat transfer enhancement in both kinds of nanofluids by increasing the volume fraction of particles as well as Peclet number. Although $Al_2O_3$-water nanofluid showed the more heat transfer enhancement than that of CuO -water in high concentrate ratio, both had roughly the same heat transfer coefficient at low concentration ratios because their thermal conductivity were close to each other.

Recently, a multi-wall nanotube in oil suspension (MWNT) yielded an extremely large increase in thermal conductivity (up to a 150% over the conductivity of oil) at 1 vol.% nanotubes [50]. This is the highest thermal conductivity enhancement ever achieved in a liquid.

In case of numerical studies of heat transfer coefficient all investigations can be categorized in two groups. The first one is called homogeneous modeling and the second is two-phase model. In the homogeneous single-phase model the effective thermo-physical properties such as conductivity, viscosity, heat capacity and density are taken into account for the whole mixture of nanoparticles and the base fluid. In addition, the particles and fluid are supposed to be in the complete chemical, thermal and hydrodynamic equilibriums. The more proper effective properties are selected, the more precise results can be obtained. In contrast, in two-phase model the particles and the fluid are distinguished as two separated phases with different thermo-physical properties. In this model the Eulerian or Lagrangian framework can be used. In the Eulerian/Eulerian framework, each phase is treated as an interpenetrating continuum having separate transport equations while in Lagrangian framework the specific particles are traced as a discrete phase. The inter-phase interactions of particles and fluid are accounted in this

way. Most of the numerical studies in this field are based on the single-phase approach (e.g. Koo et al. [51]; Li et al. [52]; Santra et al[53].

Maiga et al [54] offered a numerical formulation for study of forced convective heat transfer of $Al_2O_3$-water and $Al_2O_3$-ethylene glycol nanofluids inside a heated tube. Based on the single phased model used in this study, heat transfer increased with increasing particle volume fraction. $Al_2O_3$-ethylene glycol also showed higher heat transfer enhancement than $Al_2O_3$-water.

There are a few studies that used two-phase approach to study nanofluids. Behzadmehr et al.[55] utilized a two-phase mixture model to investigate turbulent forced convection of nanofluid inside the pipe based on thermal equilibrium assumption (the same temperatures for both particle and fluid). In comparison with the experimental works they presented that the results of two-phase model are more precise than that of the homogeneous model. Mirmasoumi and Behzadmehr [56] investigated the mixed convection of the nanofluid in a tube with the same two-phase method utilized by Behzadmehr et al. [55]. The nanoparticle size effect on the mixed convective heat transfer of a nanofluid were assessed by Mirmasoumi et al. [57] and Akbarinia et al. [58]. The two-phase mixture method were used in these numerical studies. According to both studies, heat transfer enhancement is appeared as the size of nanoparticle decreases. The nanofluid flow and heat transfer inside a pipe were simulated by Bianco et al. [59]. They employed both homogeneous single-phase and two-phase models. Among two-phase models the Lagrangian method was used to track the motion of particle. They presented that there is a maximum difference of 11% between the single and two-phase predictions. Three different homogeneous, Eulerian–Lagrangian and mixture methods are used by Kurowski et al. [60] for simulation of nanofluid flow inside a minichannel. As their results, all three methods had the same behavior approximately. The nanofluid heat transfer inside a tube was simulated by Fard et al. [61] in both the single and two-phase

approaches. For a 0.2% Cu–water nanofluid, they showed that the average relative deviation between the experimental data and single-phase model was 16% whereas for the two-phase method it was 8%. Lotfi et al. [62] also applied the three methods of homogeneous, two-phase Eulerian and mixture for nanofluid flow inside a tube. They found that among these approaches, the two-phase mixture method gives more accurate results than others.

## 2.5 Summary of literature study

According to the literature, firstly there are many studies about modeling the effective conductivities of nanofluids. Among all studies the effects of Brownian motion, nanolayer, particles volume fraction and clustering have been pronounced as the major mechanisms repeatedly. Similarly, in case of effective viscosity models, the most of studies considered particles concentration as a main parameter that influences the nanofluids viscosity. Roughly all thermal analysis shows an enhancement in heat transfer efficiency by suspension of nanoparticles in fluids. The heat transfer sensitivity to size, type, fraction and shape of particles were assessed numerically and experimentally. In many numerical studies the homogeneous single phase approximation were used to predict the measure of heat transfer. In comparison to experimental works some studies presented that the single-phase approach under-estimates the heat transfer enhancement. So, the two-phase modeling can be an alternative method. In scope of existing studies for the two-phase method, there are a few investigations that considered the temperature difference between the phases. Although the turbulence flow regime is the most common case in industry, because of complexity a few numerical studies accounted this flow regime.

# 3 Methodology

## 3.1 Introduction

Between two general data capture approaches in mechanical phenomena, experimental and numerical approach, the second one is adopted in this study. The data in thermal-fluid analysis are usually velocity, pressure and temperature. Since the main goal of simulation in this study is Nusselt number prediction, once the temperature distribution is found, the Nusselt number can by calculated by post-processing. Accordingly the initial information of the problem such as geometry, dimensions, input and initial values, dependent and independent variables of the study is determined. Then based on reliable assumptions, the geometry for the simulation is simplified. For finding velocity, pressure and temperature, the mass, momentum and energy partial deferential equations, known as governing equations must be formed and discretized by prepared commercial ANSYS-Fluent codes based on FVM method. So it needs the geometry is divided into many finite divisions or cells using meshing process. All the process described till now are referred to as the pre-processing steps. After that, when the governing equations are discretized by the software, the governing equations are converted into algebraic equations. Following that, the discretized governing equations are solved using iterative algorithms. The convergence residual and the problem initialization are specified in the simulation. This process is done through the solution part of the software. Figure 3-1 illustrates solution processes in numerical methods step by step.

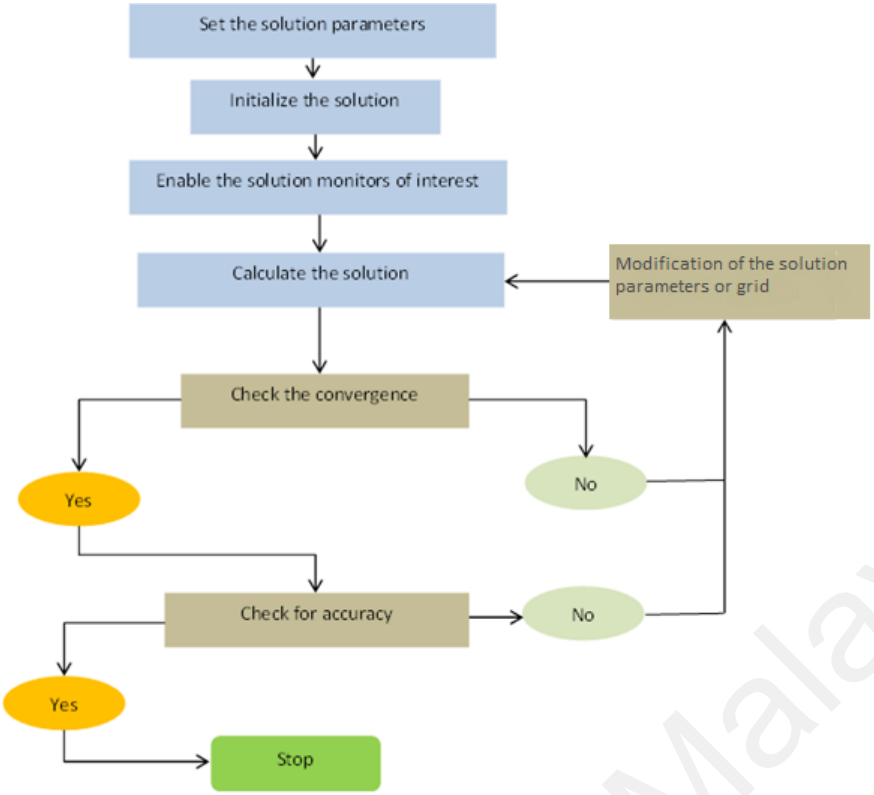


**Figure 3-1: The schematic flow chart that depicts different steps of solving process [63].**

Ultimately, it comes to post-processing step when the proper results are obtained. The accuracy of results can be checked by several methods, for example the net mass flux or heat flux in and out the control volume in post-processing panel of the software. By finding the temperature contours, the Nusselt number can be calculated by the formula in the literatures. Figure 3-2 illustrates different steps of numerical studies step by step. In next sub-chapters the details of each steps will be explained.

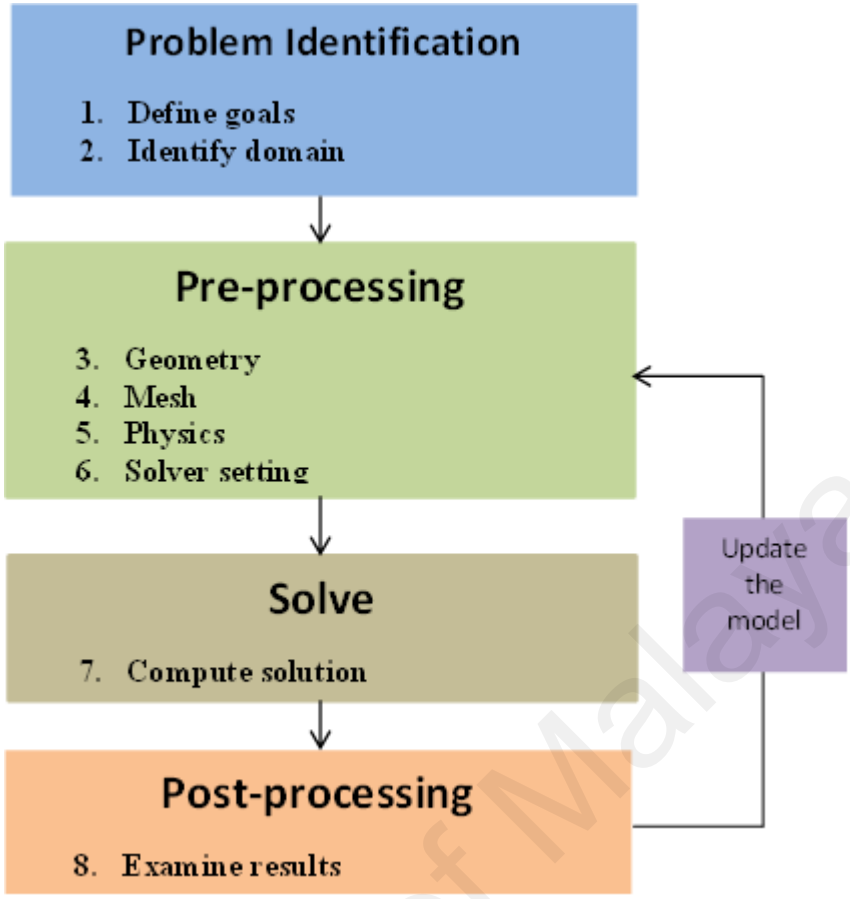


**Figure 3-2: schematic flowchart of typical steps should be done during numerical studies [63].**

## 3.2 Geometrical Structure

The cylindrical tube with uniformly heated wall is analyzed in this study. The cylindrical pipe has 0.01m diameter and 1m length. The constant heat flux applied to pipe wall. Due to the symmetrical similarity of geometry, the two-dimensional axisymmetric geometry has been taken into account. Therefore, the analysis is carried out using a rectangle domain with $0.005 \times 1$ $m^2$ dimensions.

## 3.3 Simulation Cases

A constant heat flux of $35000 W/m^2$ is applied at pipe walls. The effects of two dimensionless parameters, volume fraction ($\varphi$) of nanofluid (water-Cu) and Reynolds number (Re) are investigated. Since the simulation results are evaluated by the

experimental ones, the range of volume fraction and Reynolds number are selected the same as Xuan and Li experiment and are given as below:

- Reynolds number from 10000 to 25000
- Typical volume fractions are 0,0.3,0.5,0.8,1,1.2 and 1.5%

### 3.4 Mesh

Turbulent flows are influenced by no-slip conditions in wall-bonded problems. Obviously, the velocity field undergoes the remarkable changes due to the wall presence. Although these effects do not play crucial role somewhere far from the wall, the viscous damping and kinematic blocking reduces the tangential and normal fluctuations in the near –wall region.

It is in the near-wall region that the solution variables have a large gradient. Therefore, an accurate representation of the flow in the near-wall region determines successful predictions of wall-bounded turbulent flows. The standard k-ε model primarily is valid for turbulent core flows (i.e., the flow in the regions somewhat far from walls). Consideration therefore needs to be given as to how to make these models suitable for wall-bounded flows.

Numerous experiments have shown that the near-wall region can be largely subdivided into three layers. In the innermost layer, called the ``viscous sub-layer", the flow is almost laminar, and the (molecular) viscosity plays a dominant role in momentum and heat or mass transfer. In the outer layer, called the fully-turbulent layer, turbulence plays a major role. Finally, there is an interim region between the viscous sub-layer and the fully turbulent layer where the effects of molecular viscosity and turbulence are equally important. Figure 3-3 illustrates these subdivisions of the near-wall region, plotted in semi-log coordinates based on dimensionless velocity versus dimensionless distance.

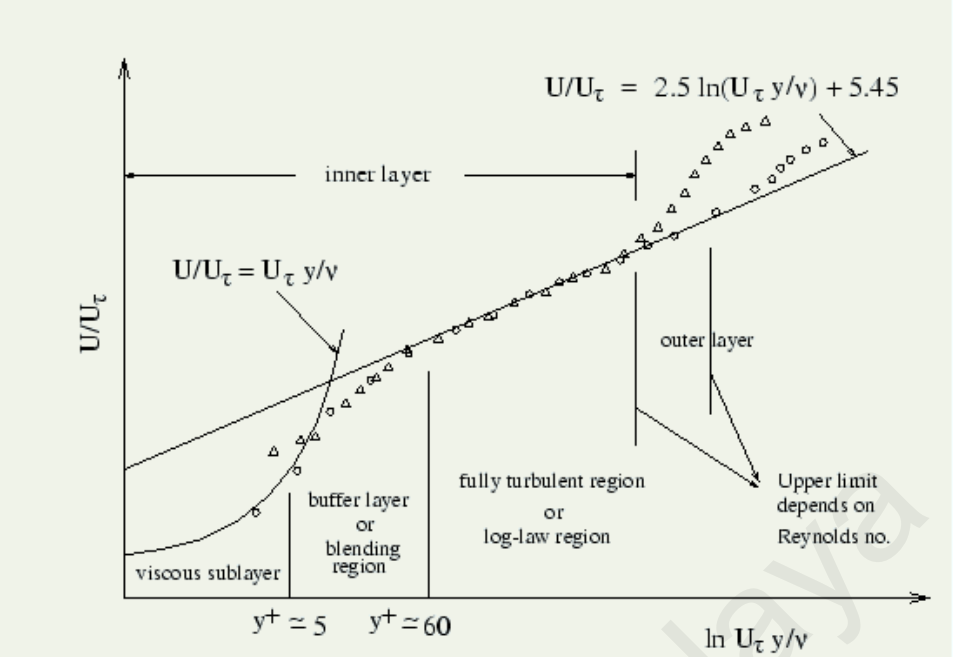


**Figure 3-3: Subdivision of the Near-Wall Region [63].**

The dimensionless velocity and distance are defined as follows:

$$u^+ = \frac{u}{u_\tau},\ y^+ = \frac{\rho u_\tau y}{\mu} \qquad \textbf{3-1}$$

where u, ρ, μ and y are velocity, density, viscosity and the normal distance from the wall respectively. The uτ is called friction velocity and defined as below:

$$u_\tau = \sqrt{\frac{\tau_w}{\rho}} \qquad \textbf{3-2}$$

where $\tau_w$ is wall shear stress.

Totally, there are two approaches for modeling near-wall region. One of it ignores viscosity-affected inner region (viscous sub-layer and buffer layer) and some semi-empirical correlations are used to make the viscosity-affected region as a link between the wall and the fully developed region. The second approach involves solving both low-Re and high-Re turbulence flows by simulation of both inner and fully turbulent regions using a denser mesh near the wall. These two approaches are depicted schematically in Figure 3-4. Enhanced wall treatment is a near-wall modeling method used by Fluent.

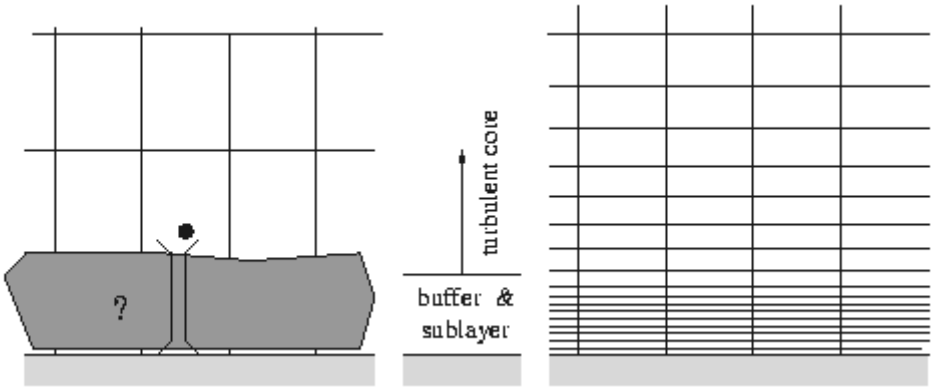


**Figure 3-4: Schematically comparison between two approaches for modeling near wall region [63].**

## 3.5 Mathematical Modeling

Numerical simulation has been used in this study. This approach gives velocity, pressure and temperature distribution from the solutions of governing equations (conservation equations). The suitable transport equation is written for conservation of mass, momentum and energy in integral form. Then the integral equations are discretised (converted to algebraic equations) by Finite Volume Method (FVM). According to an appropriate meshing and boundary condition, the algebraic equations are solved iteratively.

## 3.6 Governing Equations

Since in turbulent regime the flow properties fluctuate instantly, the time-averaged Reynolds approach (RANS) is used for governing equations. Considering the forced convection, steady state, incompressible, Newtonian and turbulent the governing equations can be derived as follows:

**Continuity equation**

$$\nabla.\overline{V} = 0 \qquad \textbf{3-3}$$

where the continuity equation has the same appearance for both single and two-phase model, although it is divided into two equations, for two-phase model, one for solid particles and another for base fluid.

**Momentum equations**

For single phase one can write:

$$\rho_{eff}(\bar{V}.\nabla\bar{V}) = -\nabla\bar{P} + \mu_{eff}\nabla^2\bar{V} - \rho_{eff}\overline{\nabla.V'V'} \quad \textbf{3-4}$$

**Conservation of energy**

$$div(\bar{T}\bar{V}) = \frac{k_{eff}}{\rho_{eff}c_{p,eff}}div(grad(\bar{T})) - (\overline{V'T'}) \quad \textbf{3-5}$$

**Standard k-ε model**

The standard k-ε model is employed according Launder et al.[64] study:

$$div(\rho_{eff}kV) = div[(\mu_{eff} + \frac{\mu_t}{\sigma_k})grad(k)] + G_k - \rho_{eff}\varepsilon \quad \textbf{3-6}$$

$$div(\rho_{eff}\varepsilon V) = div[(\mu_{eff} + \frac{\mu_t}{\sigma_\varepsilon})grad(\varepsilon)] + C_{1\varepsilon}\frac{\varepsilon}{k}G_k - C_{2\varepsilon}\rho_{eff}\frac{\varepsilon^2}{k} \quad \textbf{3-7}$$

$$G_k = -\rho_{eff}\overline{v_i'v_j'}(\nabla V),\ \mu_t = \rho_{eff}C_\mu\frac{k^2}{\varepsilon} \quad \textbf{3-8}$$

$$C_\mu = 0.09, \sigma_k = 1.00, \sigma_\varepsilon = 1.30, C_{1\varepsilon} = 1.44, C_{2\varepsilon} = 1.92$$

On the other hand for Eulerian-Eulerian two-phase flow the equations can be written as:

**Conservation of momentum**

$$\rho_l(\bar{V}.\nabla\bar{V}) = -\varphi_l\nabla\bar{P} + F_d + \mu_l\nabla^2\bar{V} - \rho_l\overline{\nabla.V'V'} \quad \textbf{3-9}$$

$$\rho_p(\bar{V}.\nabla\bar{V}) = -\varphi_p\nabla\bar{P} - F_d + \mu_p\nabla^2\bar{V} - \rho_p\overline{\nabla.V'V'} \quad \textbf{3-10}$$

$$\varphi_l + \varphi_p = 1 \quad \textbf{3-11}$$

where the l and *p* subscriptions represent the liquid and particle properties respectively. The drag force is also the only body force considered. Since the gravitational force in r

direction is so small relative to high virtual inertia force (turbulent effects), it is neglected. In addition to this the added mass and particle-particle interaction forces are negligible according to dilute mixture flow.

The drag force between the phases is calculated by Equation 3-12 as:

$$F_d = \beta(\vec{V}_l - \vec{V}_p) \quad \textbf{3-12}$$

The friction coefficient $\beta$ is calculated according to the particle volume concentration range. The drag coefficient offered by Schiller-Naumann [65] is used by Equation 3-13 in this study as follows:

$$\beta = \frac{3}{4}\frac{C_D}{d_p}\varphi_p \rho_l \left|V_l - V_p\right| \quad \textbf{3-13}$$

$$C_D = \frac{24}{\mathrm{Re}_p}(1 + 0.15\,\mathrm{Re}_p{}^{0.687}) \quad \textbf{3-14}$$

where

$$\mathrm{Re}_p = \frac{\varphi_l \rho_l \left|\vec{V}_l - \vec{V}_p\right| d_p}{\mu_l} \quad \textbf{3-15}$$

**The standard k-ε model**

The standard K-Ɛ model is employed according to Launder et al.[64] study for each phase individually:

$$div(\varphi_l \rho_l k_l V_l) = div[(\mu_l + \frac{\varphi_l \mu_{t_l}}{\sigma_k}) grad(k_l)] + \varphi_l G_k - \varphi_l \rho_l \varepsilon_l \quad \textbf{3-16}$$

$$\frac{\partial(\varphi_l \rho_l \varepsilon_l)}{\partial t} + div(\varphi_l \rho_l \varepsilon_l V_l) = div[\frac{\varphi_l \mu_{t_l}}{\sigma_\varepsilon} grad(\varepsilon_l)] + \varphi_l C_{1\varepsilon} \frac{\varepsilon_l}{k_l} 2\mu_{t_l} S_{ij_l} . S_{ij_l} - \varphi_l C_{2\varepsilon} \rho_l \frac{\varepsilon_l{}^2}{k_l} \quad \textbf{3-17}$$

$$\frac{\partial(\varphi_p \rho_p k_p)}{\partial t} + div(\varphi_p \rho_p k_p V_p) = div[\frac{\varphi_p \mu_{tp}}{\sigma_k} grad(k_p)] + 2\varphi_p \mu_{t_p} S_{ij_p}.S_{ij_p} - \varphi_p \rho_p \varepsilon_p \quad \textbf{3-18}$$

$$\frac{\partial(\varphi_p \rho_p \varepsilon_p)}{\partial t} + div(\varphi_p \rho_p \varepsilon_p V_p) = div[\frac{\varphi_p \mu_{t_p}}{\sigma_\varepsilon} grad(\varepsilon_p)] + \varphi_p C_{1\varepsilon} \frac{\varepsilon_p}{k_p} 2\mu_{t_p} S_{ij_p}.S_{ij_p} - \varphi_p C_{2\varepsilon} \rho_p \frac{\varepsilon_p^{\,2}}{k_p} \quad \textbf{3-19}$$

$$C_\mu = 0.09, \sigma_k = 1.00, \sigma_\varepsilon = 1.30, C_{1\varepsilon} = 1.44, C_{2\varepsilon} = 1.92$$

Where k and Ɛ represent are the turbulent kinetic energy and turbulent dissipation rate respectively.

**Conservation of energy**

Considering the base fluid and the particle phase as incompressible fluids, and neglecting the viscous dissipation and radiation, the energy equation is written as

$$\varphi_l(div(\bar{T}\bar{V})) = \frac{k_{eff,l}}{\rho_l c_{p,l}} div(\varphi_l grad(\bar{T}_l)) - \varphi_l(\overline{V'T'}) - h_v(\bar{T}_l - \bar{T}_p) \quad \textbf{3-20}$$

$$\varphi_p(div(\bar{T}\bar{V})) = \frac{k_{eff,p}}{\rho_p c_{p,p}} div(\varphi_p grad(\bar{T}_p)) - \varphi_p(\overline{V'T'}) + h_v(\bar{T}_l - \bar{T}_p) \quad \textbf{3-21}$$

where $C_p$, T, $k_{eff}$ and $h_v$ are the heat capacity at constant pressure, temperature, effective thermal conductivity and volumetric interphase heat transfer coefficient, respectively. For mono-dispersed spherical particles $h_v$ can be calculated from

$$h_v = \frac{6(1-\varphi_l)}{d_p} h_p \quad \textbf{3-22}$$

where $h_p$ is the fluid–particle heat transfer coefficient that should be calculated from empirical correlations. In the present study the fluid–particle heat transfer coefficient is calculated based on the Equation 3-23 offered by the Whitaker [66].

$$Nu_p = 2 + (0.4\,\mathrm{Re}_P^{1/2} + 0.06\,\mathrm{Re}_D^{2/3})\,pr^{0.4}$$
$$0.71 \le \mathrm{Pr} \le 380 \qquad \textbf{3-23}$$
$$3.5 \le \mathrm{Re}_p \le 7.6\times10^4$$

Here Pr is the base liquid Prandtl number.

For finding the details of governing equation for both single and two-phase models based on different phases or direction components the more information have been offered in appendix A.

## 3.7 Physical Properties of Nanofluid

### 3.7.1 Single Phase

As a first estimation it can be taken into account the single phase fluid with the effective thermo-physical properties. This means the mixture of fluid and suspended nano solid particles are considered as a unique fluid but with the different properties from the base fluid. Additionally, the mixture is supposed under chemical and physical equilibrium. In other words there are no thermal, chemical and hydrodynamic interaction between fluid and particles. Hence it is recommended the effective properties for homogeneous mixture of solid-liquid.

The effective mass density of the nanofluid $\rho_{eff}$ is given by:

$$\rho_{eff} = (1-\varphi)\rho_f + \varphi\rho_s \qquad \textbf{3-24}$$

where $\rho_f$ and $\rho_s$ are the mass densities of the base fluid and the solid nanoparticles, respectively.

The heat capacity at constant pressure per unit volume of the nanofluid $(\rho c)_{eff}$ is:

$$(\rho c_p)_{eff} = (1-\varphi)(\rho c_p)_f + \varphi(\rho c_p)_s$$
, **3-25**

where c is the specific heat at constant pressure, and $(\rho c)_f$ and $(\rho c)_s$ are the heat capacities at constant pressure per unit volume of the base fluid and the solid nanoparticles, respectively. Accordingly, the effective specific heat at constant pressure of the nanofluid $C_{eff}$ is calculated as:

$$c_{p,eff} = \frac{(1-\varphi)(\rho c_p)_f + \varphi(\rho c_p)_s}{(1-\varphi)\rho_f + \varphi\rho_s} \quad \textbf{3-26}$$

For effective viscosity and conductivity the experimental measures used by Li et al. [48] are employed in this study. Table 3-1 shows the corresponding data of nanofluid conductivity and viscosity at different particle concentrations.

**Table 3-1: The effective thermal conductivity and viscosity of Cu-water nanofluid [48]**

| Cu/water nanofluids properties | | |
|---|---|---|
| ϕ(Volume fraction) | $K_{nf}$(W/m.$^0$C) | $\nu_{nf \times 10^6}$(m$^2$/s) |
| 0.3% | 0.6054 | 0.91 |
| 0.5% | 0.615 | 0.915 |
| 0.8% | 0.6252 | 0.945 |
| 1% | 0.6306 | 0.96 |
| 1.2% | 0.633 | 1.012 |
| 1.5% | 0.663 | 1.044 |

### 3.7.2 Eulerian-Eulerian Two-Phase Model

In the Eulerian-Eulerian model the nanofluid is supposed as a mixture of two continuum fluids. Accordingly two sets of governing equations, one for particles and the other for liquid, must be written. Additionally the effects of particle-fluid interactions are considered by this approach. Based on this model the physical properties of water are taken into account for liquid phase, except for conductivity calculated by Kuipers et al.[67] correlations. The physical properties of particles phase equations are corresponded to copper properties except for conductivity calculated by Kuipers et al. correlations. In addition the solid viscosity of particles is assumed as water viscosity due to reference [65].

The effective thermal conductivities for liquid and particle phases are estimated by Kuipers et al.[67] correlations, Equations 3-27 and 3-28, as:

$$k_{eff,l} = \frac{k_{b,l}}{\varphi_l} \quad \textbf{3-27}$$

$$k_{eff,p} = \frac{k_{b,p}}{\varphi_p} \quad \textbf{3-28}$$

where

$$k_{b,l} = (1-\sqrt{(1-\varphi_l)})k_l \quad \textbf{3-29}$$

$$k_{b,p} = (\sqrt{(1-\varphi_l)}(\omega A + |1-\omega|\Gamma)k_l \quad \textbf{3-30}$$

and

$$\Gamma = \frac{2}{(1-\frac{B}{A})}\left\{\frac{B(A-1)}{A(1-\frac{B}{A})^2}\ln(\frac{A}{B}) - \frac{(B-1)}{(1-\frac{B}{A})} - \frac{B+1}{2}\right\} \quad \textbf{3-31}$$

with

$$A = 1.25(\frac{[1-\varphi_l]}{\varphi_l})^{\frac{10}{9}}$$

$$B = \frac{k_p}{k_l} \quad \textbf{3-32}$$

$$\omega = 7.26\times10^{-3}$$

Although Equations (3-27) to (3-32) are not developed for nano-sized particles, since there is not any correlation for nanofluids, these relations are considered for the first estimation.

### 3.8 Numerical Method

A steady-state solution and a segregated method are taken into account to solve the set of nonlinear governing equations. A second-order upwind scheme for the momentum, turbulent kinetic energy and turbulent dissipation rate equations are selected whereas the

first order upwind for energy equation is selected. All these conditions are the same for governing equations of both single and multiphase model except for the volume fraction correlation, which is added to the multiphase equation and solved by first order scheme. The SIMPLE coupling algorithm is selected for single phase in order to couple pressure and velocity. For Eulerian multiphase calculations, the phase momentum equations, and the phasic volume fraction equations with the shared pressure are solved in a coupled and segregated fashion. After solving the equations in a segregated manner, the phase coupled SIMPLE (PC-SIMPLE) algorithm is employed for the pressure-velocity coupling. PC-SIMPLE is an extension of the SIMPLE algorithm to multiphase flows. The velocities are solved coupled by phases, but in a segregated fashion. The scaled residuals for the velocity components and energy are set equal to $10^{-3}$ and $10^{-6}$, respectively.

### 3.9 Boundary conditions

For single phase method, the boundary conditions are as below:

- At the pipe inlet (z=0):

$$v_z = u_0,\ v_r = 0,\ T = T_0, I = I_0 \qquad \textbf{3-33}$$

and based on turbulent intensity definition one can write:

$$k_0 = \frac{3}{2}(I_0 u_0)^2 \qquad \textbf{3-34}$$

- At the wall (r=D/2):

$$v_z = v_r = 0,\ \text{k}=\varepsilon=0,\ q_w'' = -k_{eff}\frac{dT}{dr} \qquad \textbf{3-35}$$

- At symmetric axis (r=0):

$$\frac{dT}{dr} = \frac{dv_r}{dr} = \frac{dv_z}{dr} = 0 \qquad \textbf{3-36}$$

The pressure outlet boundary condition is considered at pipe exit (z=L).

For Eulerian-Eulerian two-phase flow all above conditions are chosen for both phases. Additionally, the velocity of particles is assumed the same as that of fluid at pipe inlet.

# 4 Results and Discussion

## 4.1 Mesh Dependency Study

Since the enhanced wall treatment model is selected for this case study, $y^+$ value of the first mesh node in the k-ε turbulence model is checked and is recommended to be lower than 5 [63]. A mesh need to be dense near the wall where the effect of viscosity is so high but the turbulent mechanism is low. Figure 4-1 shows the schematic of the mesh type in this study. Accuracy of the enhanced wall treatment model is assessed and shown in Figure 4-2. The $y^+$ value for the most of cells near the wall is on average about 2. Hence this shows that the enhanced wall function meets the satisfactory requirements of the wall function.

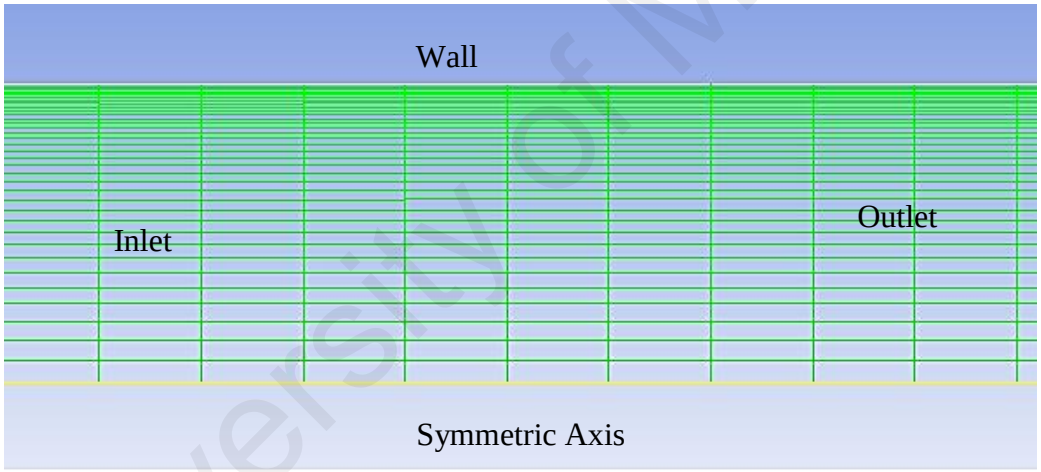


**Figure 4-1: Meshing type adopted in this study, it is dense near the wall while the mesh becomes coarse as closing the symmetric axis**

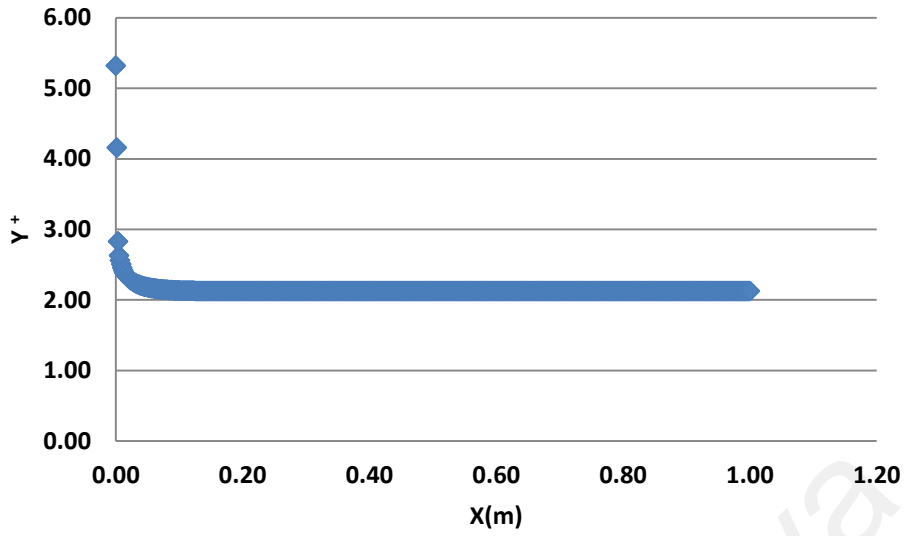


**Figure 4-2: The measure of $Y^+$ at different X position on the wall**

Several different grids have been tested based on turbulent forced convection of water flow to ensure that the calculated results are grid independent. Figure 4-3 shows the velocity profiles, temperature profiles and Nusselt numbers versus Reynolds numbers for three different grids. All these grids give the same results. The selected grid in this study consists of 600 and 35 nodes in the axial and radial directions, respectively.

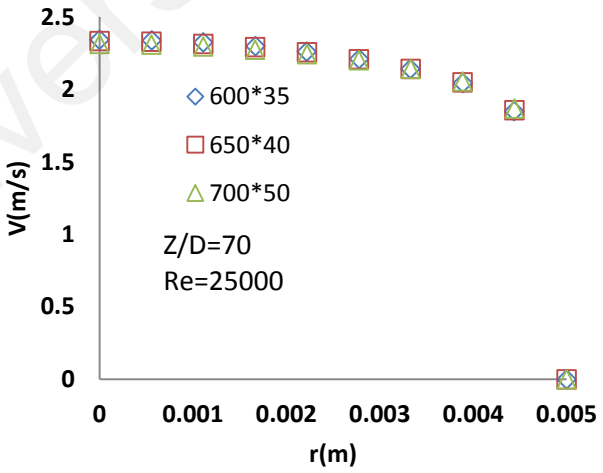


a)

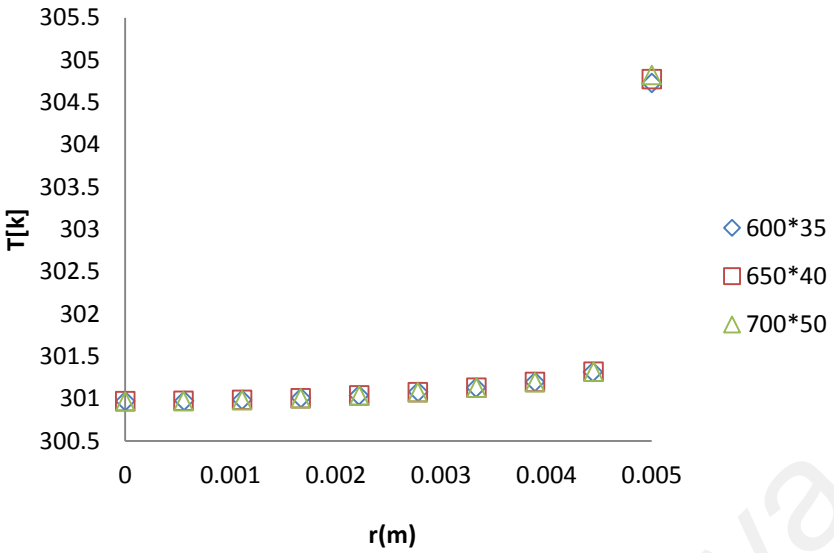


b)

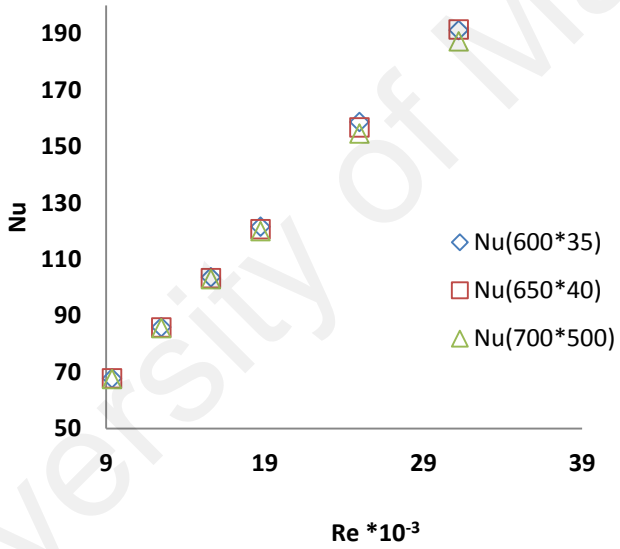


**Figure 4-3: Mesh dependency test results based on water**



## 4.2 Validation

The numerical approach used in this study to investigate the turbulence forced convection flow through a cylindrical pipe is checked and validated in this section. For this, pure water (φ=0) flow is simulated under different high Reynolds numbers with a constant

wall heat flux. The length of pipe used is sufficiently long in order to achieve a fully developed turbulent flow regime. The results of the simulation are compared with Dittus-Boelter and Gnielinski [68] correlations, which are reliable for case of developed turbulent forced convection.

Figure 4-4, which shows the Nusselt number versus the Reynolds number, compares the simulation predictions from this study with Xuan and Li [48] experiment results, Dittus-Boelter and Gnielinski correlation values for pure water. The simulation predictions have a close coincidence to the experimental results of Xuan and Li. Nusselt numbers of the simulation between Re=10000 to 19000, are quite consistent with the two correlations. For Reynolds number more than 19000, some differences can be seen between the simulation and the correlations. As an overall, the simulation gives an accurate Nusselt number as that of the correlations up to Re=19000 with the difference less than 2%. But after Re=1900 this deviation reaches about 6% at about Re= 25000 for Dittus-Boelter correlation. For Re>19000, the simulation results are closer to Gnielinski correlation with the difference about 4% everywhere. Since the Dittus-Boelter equation can be used for small to moderate temperature differences between the tube wall and the fluid at inlet, according to the literature the Dittus-Boelter equation is less precise than Gnielinski correlation at high Reynolds numbers.

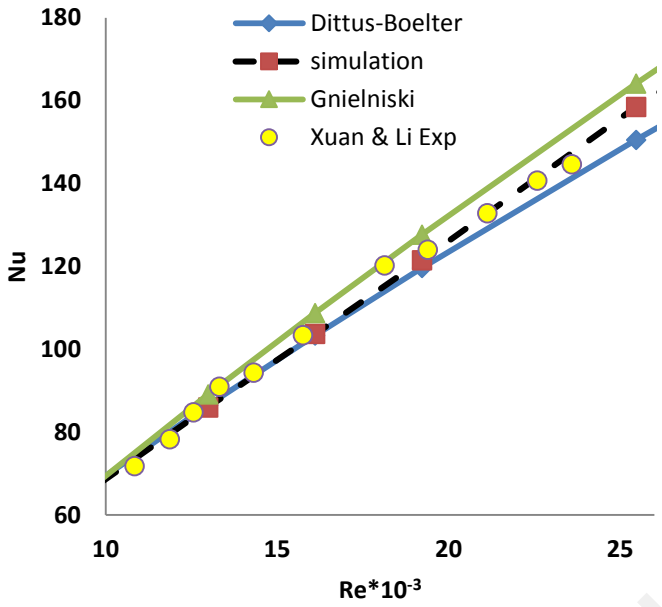


**Figure 4-4: Comparison of the predicted Nusselt numbers of water by simulation with Xuan and Li experiment, the calculated values from Dittus-Boelter and Gnielniski equations**

## 4.3 Single Phase Model

The turbulent forced convection of nanofluid inside a heated tube has been simulated by using a single-phase model in this study. Nusselt numbers are calculated at different Re number and particle fractions. Then the results of the simulation are compared with Xuan and Li [48] experimental results for accuracy assessment. Table 4-1 shows the Nusselt number of Cu-water nanofluid at Reynolds numbers of 10000 to 25000 and copper nanoparticle volume fractions of 0.3%, 0.5%, 0.8%, 1%, 1.2% and 1.5%. The values of Nusselt number calculated by the Li et al.[48] correlation is also included. The red marker points represent Nusselt numbers based on the simulation results. The result for 0.5% volume fraction has the highest difference with Xuan and Li correlation. As the volume fraction increases, the error reduces and 1.2% volume fraction has the least difference. However, at the volume fraction of 1.5%, the simulation results show the deviation from

the experimental data again. The simulation under-predicts the Nusselt numbers for 1.5% volume fraction but it overestimates for the other volume fractions.

As a result, the single phase model is not able to predict precisely the Nusselt number for all volume fractions. For example, it predicts a reasonable Nusselt numbers at some volume fractions such as 1, 1.2 and 1.5%. However it is not accurate for 0.3, 0.5 and 0.8% volume fractions, which show more than 10% deviation as shown in Figure 4-5. In addition the simulation results show the over-prediction of Nusselt number in the all cases except for the fraction of 1.5% that shows under-prediction of Nusselt number. Finally, in contrast of previous investigations already done through the literatures, the Nusselt numbers show the decreasing trend as volume fraction increases. Consequently, it can be concluded the single-phase model is an unreliable one for the Nusselt number prediction.

**a)**

| Single-phase model, ϕ (0.3%) | | | |
|---|---|---|---|
| **Re** | **Nu(Simulation)** | **Nu(Xuan & Li EXP)** | **Error(ɳ)** |
| **10000** | 69.46 | 85.07 | 22.47 |
| **15000** | 101.02 | 120.14 | 18.92 |
| **17000** | 113.41 | 134.40 | 18.51 |
| **18000** | 119.56 | 141.60 | 18.43 |
| **20000** | 131.78 | 155.98 | 18.36 |
| **25000** | 161.96 | 189.45 | 16.98 |

**b)**

| Single-phase model, ϕ (0.5%) | | | |
|---|---|---|---|
| **Re** | **Nu(Simulation)** | **Nu(Xuan & Li EXP)** | **Error(ɳ)** |
| **10000** | 72.74 | 85.04 | 16.92 |
| **15000** | 105.79 | 120.10 | 13.52 |
| **17000** | 118.76 | 134.36 | 13.13 |
| **18000** | 125.21 | 140.84 | 12.49 |
| **20000** | 138.01 | 155.93 | 12.98 |
| **25000** | 169.61 | 189.40 | 11.67 |

c)

| Single-phase model, ϕ (0.8%) | | | |
|---|---|---|---|
| **Re** | **Nu(Simulation)** | **Nu(Xuan & Li EXP)** | **Error(ɳ)** |
| **10000** | 77.82 | 85.75 | 10.20 |
| **15000** | 113.18 | 121.18 | 7.06 |
| **17000** | 127.06 | 135.59 | 6.72 |
| **18000** | 133.95 | 142.86 | 6.65 |
| **20000** | 147.65 | 157.39 | 6.60 |
| **25000** | 181.46 | 190.98 | 5.25 |

d)

| Single-phase model, ϕ (1%) | | | |
|---|---|---|---|
| **Re** | **Nu(Simulation)** | **Nu(Xuan & Li EXP)** | **Error(ɳ)** |
| **10000** | 80.82 | 86.05 | 6.47 |
| **15000** | 117.55 | 121.62 | 3.46 |
| **17000** | 131.96 | 136.11 | 3.14 |
| **18000** | 139.12 | 143.41 | 3.08 |
| **20000** | 153.35 | 157.99 | 3.03 |
| **25000** | 188.46 | 191.64 | 1.69 |

e)

| Single-phase model, ϕ (1.2%) | | | |
|---|---|---|---|
| **Re** | **Nu(Simulation)** | **Nu(Xuan & Li EXP)** | **Error(ɳ)** |
| **10000** | 85.08 | 87.51 | 2.86 |
| **15000** | 123.75 | 123.84 | 0.08 |
| **17000** | 138.92 | 138.66 | 0.19 |
| **18000** | 146.45 | 146.12 | 0.23 |
| **20000** | 161.43 | 161.00 | 0.27 |
| **25000** | 198.40 | 194.83 | 1.80 |

f)

| Single-phase model, ϕ (1.5%) | | | |
|---|---|---|---|
| Re | Nu(Simulation) | Nu(Xuan & Li EXP) | Error(ɳ) |
| **10000** | 88.28 | 88.20 | 0.10 |
| **15000** | 128.41 | 124.89 | 2.74 |
| **17000** | 144.15 | 139.86 | 2.98 |
| **18000** | 151.97 | 147.41 | 3.01 |
| **20000** | 167.51 | 162.42 | 3.04 |
| **25000** | 205.88 | 196.30 | 4.65 |

**Table 4-1: [a-f] :Comparison between the measured Nusselt numbers of cu-water nanofluid based on effective single phase model CFD simulation and Xuan et al. correlations**

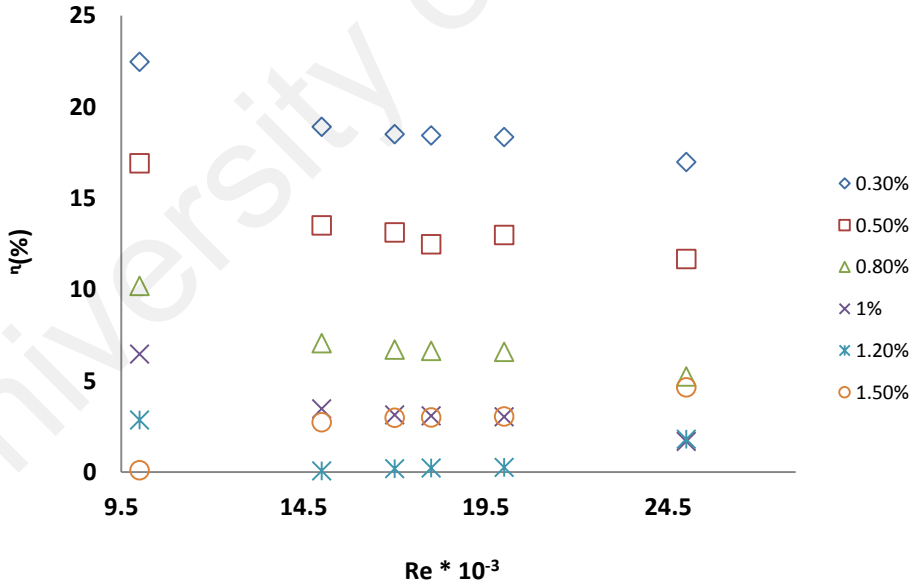


**Figure 4-5: The percentage of difference between calculated Nusselt numbers based on effective single phase model simulation and Xuan et al. correlation**

## 4.4 Two Phase Model

As discussed in Section 4.2, the single-phase CFD model is not able to predict the Nusselt number accurately. Therefore, the two-phase model which includes the interphase interaction is used for simulations. At first, Nusselt numbers are calculated at different Re numbers and particle fractions. Then results of the simulation using Eulerian-Elerian two-phase model are compared with Xuan and Li [48] experimental results for accuracy assessment. According to Table 4-2 and Figure 4-6, the Nusselt numbers of the simulations and the experimental investigations are close to each other for 0.5 % and 0.8% volume fractions with a difference of less than 10%. However, the differences are significant for the other fractions. In addition the measure of errors increases by Reynolds number in most of the cases. The simulation overestimates for 0.3%, 0.5% and 0.8% fractions, but under-predicts for the other fractions. As a result, the two-phase model is found to be inconsistent for a wide range of volume fractions, despite that this model considers the phase interactions. This comes from lack of effective nanoparticles conductivity. In next section, the two-phase model is modified to improve the prediction of Nusselt number by correction of effective particles conductivity.

**a)**

| Two-phase model, ϕ (0.3%) | | | |
|---|---|---|---|
| **Re** | **Nu(Simulation)** | **Nu(Xuan & Li EXP)** | **Error(ɳ)** |
| **10000** | 99.13 | 69.46 | 42.71 |
| **15000** | 114.31 | 101.02 | 13.15 |
| **17000** | 126.78 | 113.41 | 11.79 |
| **18000** | 133.01 | 119.56 | 11.25 |
| **20000** | 145.57 | 131.78 | 10.46 |
| **25000** | 177.44 | 161.96 | 9.56 |

**b)**

| Two-phase model, ϕ (0.5%) | | | |
|---|---|---|---|
| **Re** | **Nu(Simulation)** | **Nu(Xuan & Li EXP)** | **Error(ɳ)** |
| **10000** | 79.58 | 72.74 | 9.41 |
| **15000** | 110.53 | 105.79 | 4.48 |
| **17000** | 122.42 | 118.76 | 3.07 |
| **18000** | 128.31 | 125.21 | 2.48 |
| **20000** | 140.13 | 138.01 | 1.54 |
| **25000** | 170.27 | 169.61 | 0.39 |

**c)**

| Two-phase model, ϕ (0.8%) | | | |
|---|---|---|---|
| **Re** | **Nu(Simulation)** | **Nu(Xuan & Li EXP)** | **Error(ɳ)** |
| **10000** | 77.68 | 77.82 | 0.17 |
| **15000** | 107.76 | 113.18 | 4.79 |
| **17000** | 119.27 | 127.06 | 6.13 |
| **18000** | 124.95 | 133.95 | 6.72 |
| **20000** | 136.22 | 147.65 | 7.74 |
| **25000** | 164.77 | 181.46 | 9.19 |

**d)**

| Two-phase model, ϕ (1%) | | | |
|---|---|---|---|
| **Re** | **Nu(Simulation)** | **Nu(Xuan & Li EXP)** | **Error(ɳ)** |
| **10000** | 76.38 | 80.82 | 5.49 |
| **15000** | 105.87 | 117.55 | 9.94 |
| **17000** | 117.18 | 131.96 | 11.20 |
| **18000** | 122.74 | 139.12 | 11.77 |
| **20000** | 133.73 | 153.35 | 12.79 |
| **25000** | 161.29 | 188.46 | 14.42 |

**e)**

| Two-phase model, ϕ (1.2%) | | | |
|---|---|---|---|
| **Re** | **Nu(Simulation)** | **Nu(Xuan & Li EXP)** | **Error(ɳ)** |
| **10000** | 77.56 | 85.08 | 8.84 |
| **15000** | 107.48 | 123.75 | 13.14 |
| **17000** | 118.97 | 138.92 | 14.36 |
| **18000** | 124.61 | 146.45 | 14.91 |
| **20000** | 135.75 | 161.43 | 15.91 |
| **25000** | 163.60 | 198.40 | 17.54 |

**f)**

| Two-phase model, ϕ(1.5%) | | | |
|---|---|---|---|
| **Re** | **Nu(Simulation)** | **Nu(Xuan & Li EXP)** | **Error(ɳ)** |
| **10000** | 76.71 | 88.28 | 13.10 |
| **15000** | 106.23 | 128.41 | 17.28 |
| **17000** | 117.59 | 144.15 | 18.43 |
| **18000** | 123.17 | 151.97 | 18.95 |
| **20000** | 134.15 | 167.51 | 19.92 |
| **25000** | 161.25 | 205.88 | 21.67 |

**Table 4-2 [a-f]:Comparison between the measured Nusselt numbers of cu-water nanofluid based on Eulerian-Eulerian two -phase flow CFD simulation and Xuan et al. correlations**

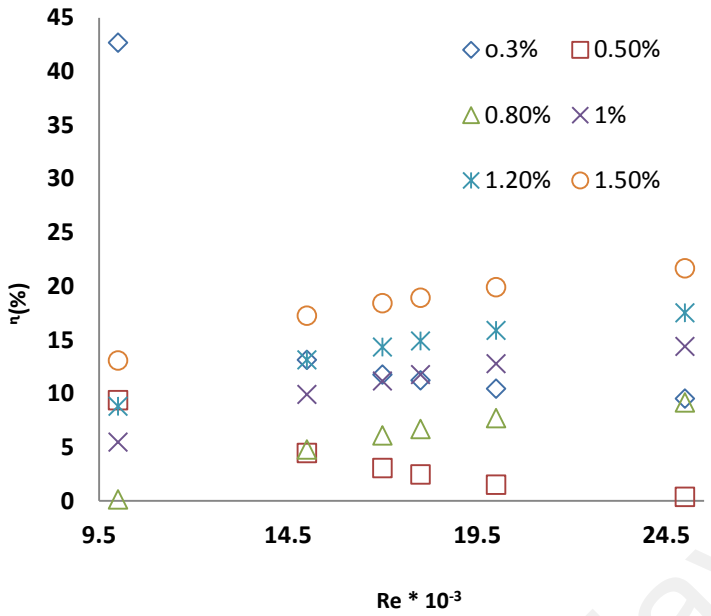


**Figure 4-6: The percentage of difference between calculated Nusselt numbers based on Eulerian-Eulerian two-phase model simulation and Xuan et al. correlation**

## 4.5 Correction Effective Particle Conductivity

The hydrodynamic and thermal diffusive terms play a significant role in the heat transfer mechanism. The viscosity and thermal conductivity are the diffuse term in momentum and energy equations, respectively. The results of the CFD simulations based on the two-phase model are improved by focusing on these two parameters. The particle viscosity is considered as water viscosity according to Kalteh et al. [65] study but a specific correlation for the effective nanoparticle conductivity is not given. According to Table 4-2 and Figure 4-6, Kuipers et al. [67] correlations were used to calculate the first assumption of a particle conductivity in the cases of this study. Following that, based on the trial and error method, an accurate copper nanoparticle conductivity, which can predict an accurate Nusselt number, has been identified for Reynolds numbers of 10000, 15000, 17000, 18000, 20000 and 25000 and volume fractions of 0.3%, 0.5%, 0.8%, 1%, 1.2% and 1.5 %. Figure 4-7 shows the values of the effective nanoparticle conductivities which give accurate Nusselt numbers. The trend lines and their correlations are also shown in

Figure 4-7. The trend-line is shown as a function between the effective particle conductivity and Re number for some volume fractions. It can be seen that the particle conductivity versus the Reynolds number has linear patterns. The value of the particle conductivity increases as the increase of the Reynolds number. In fact, an increase of velocity leads to high particle motion as well as high particles and water molecules collision. In addition, the increase motion of particles decreases the thickness of hydrodynamic viscous sub-layer. Hence, this leads to the enhancement of the effective particle conductivity. The difference of the particle conductivities for 0.3 and 0.5% fractions is large, but such difference for 1.2 and 1.5% fractions is small. The results shows that the change rate of the particle conductivity versus the Reynolds numbers is different for all volume fractions. For example, the trend-lines at 0.5, 0.8, 1.2 and 1.5% fractions have slope gradients of 0.016, 0.012, 0.015 and 0.015, respectively. In contrary, the least changes of Nusselt numbers relative to the Reynolds numbers is seen at 0.3 % fraction. In the next step, the accuracy of the developed correlations is evaluated. So, the effective particle conductivities are calculated for all six fractions at three typical Reynolds numbers of 11000, 19000, and 24000. Then the CFD simulation is carried out using Eulerian-Elerian two-phase model and the effective particle conductivity from the developed correlation in this study. Finally the results of simulation are compared to Li et al. [48] experiment results. The Figure 4-8 illustrates this comparison. Since the Nusselt numbers obtained from the simulation are close to Xuan and Li correlation, it can concluded the corresponding effective particle conductivity correlations is in good agreement.

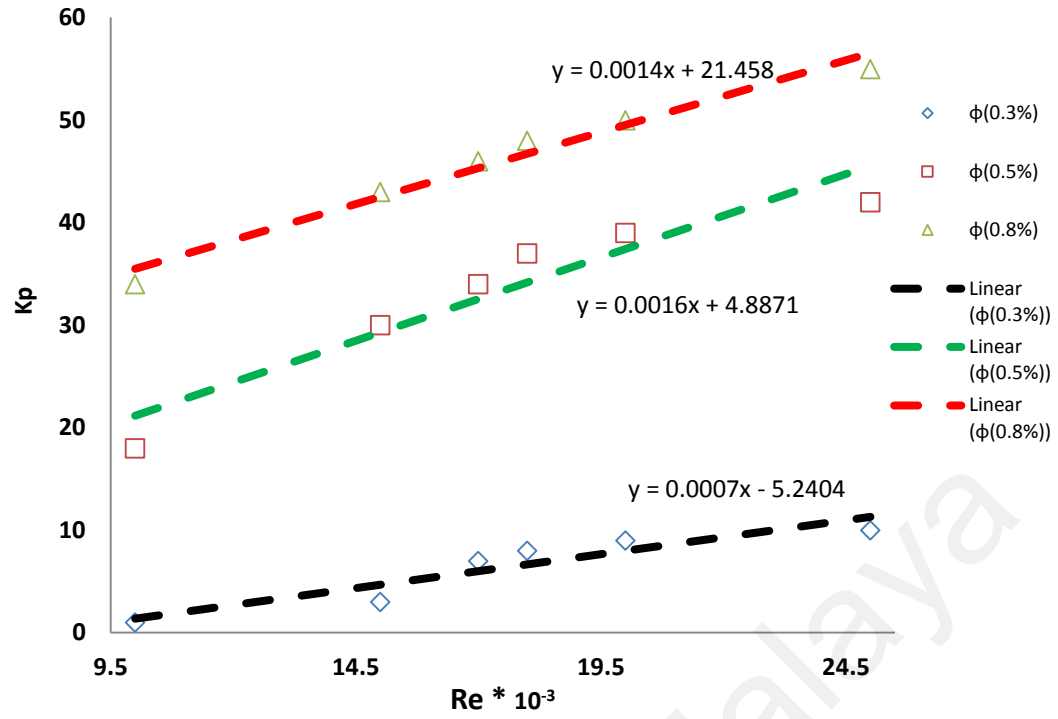


a)

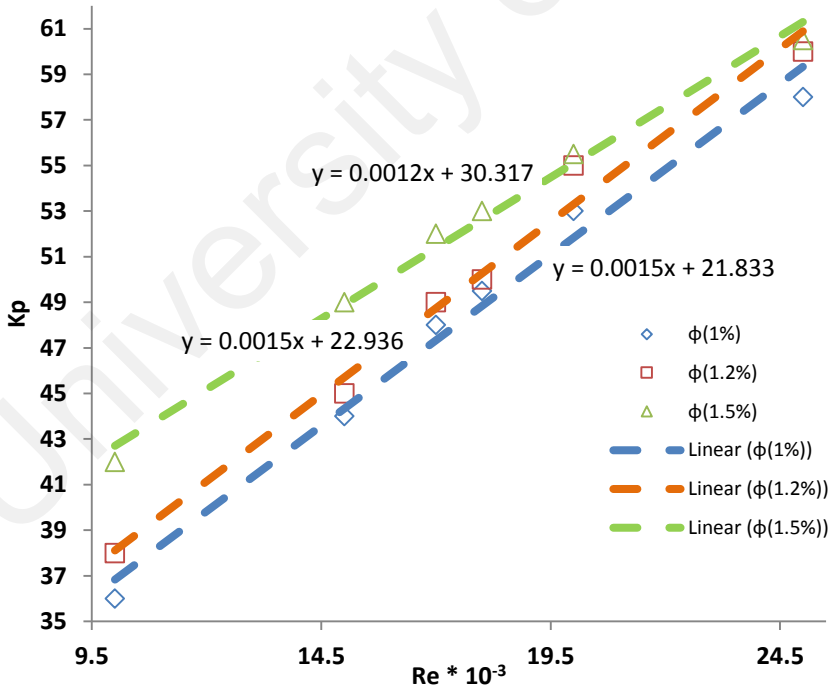


b)

**Figure 4-7 [a-b]: The effective Cu nanoparticle conductivities versus Reynolds numbers at different volume fractions according trial and error**

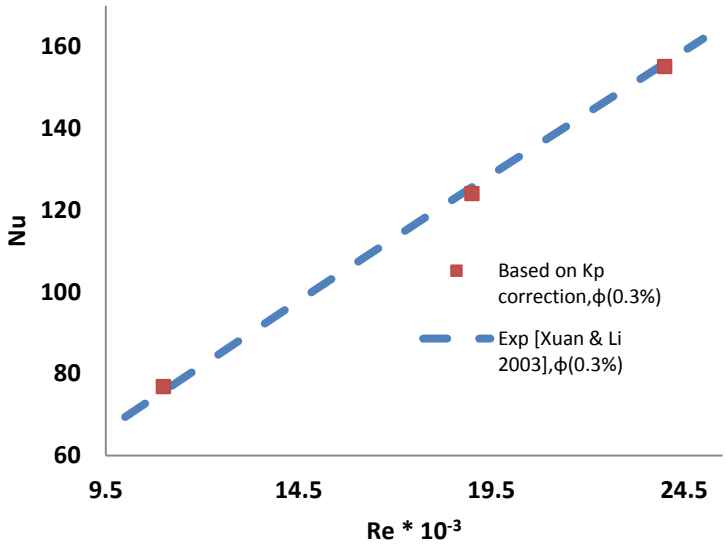


a)

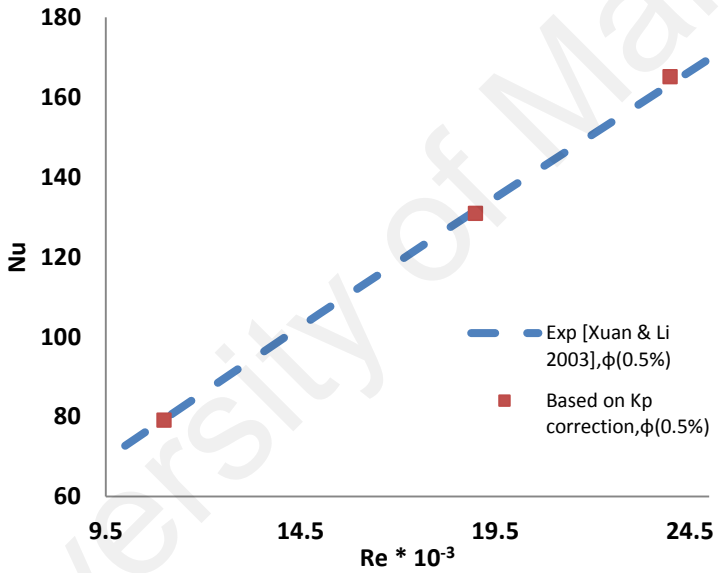


b)

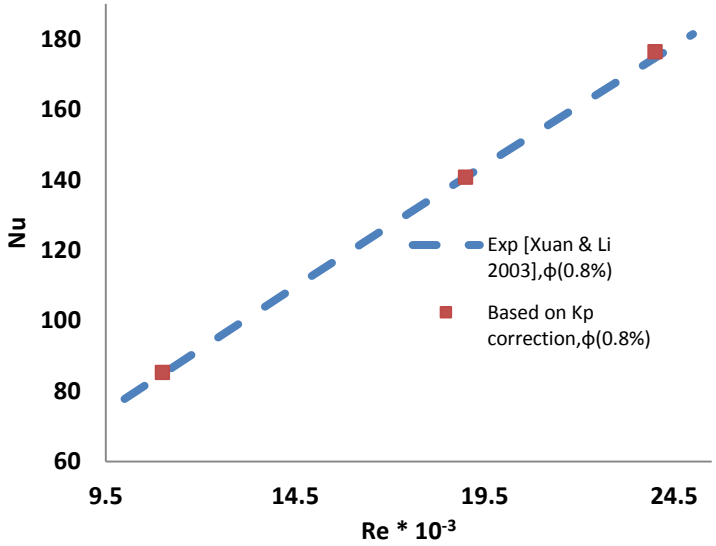


c)

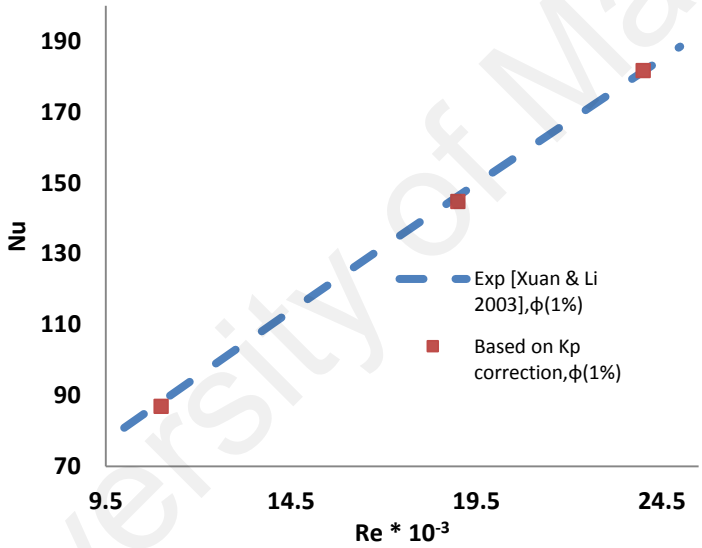


d)

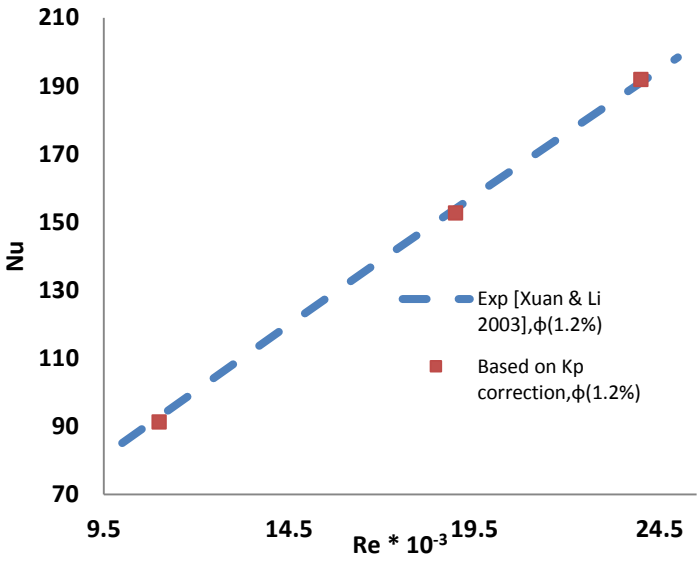


e)

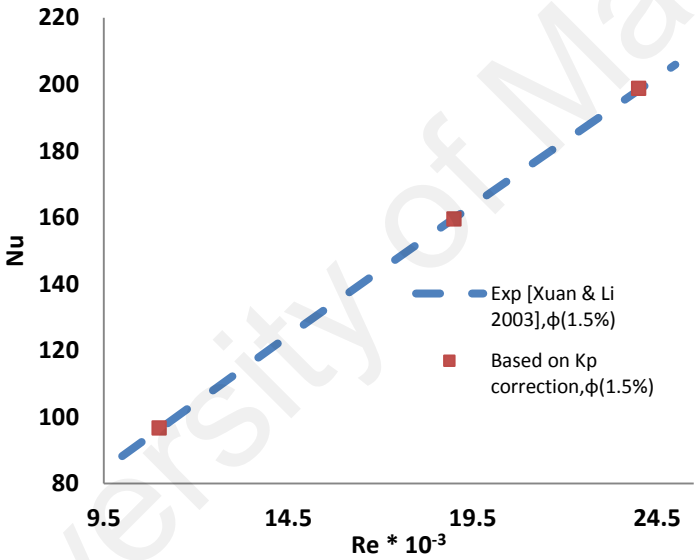


f)

**Figure 4-8 [a-f] : Validation of effective Cu nanoparticle conductivity correlations at different volume fractions and Reynolds numbers**

# 5 Conclusions

Forced convection heat transfer of Cu-water nanofluid inside a pipe with a constant wall heat flux has been investigated numerically at extended range of Reynolds numbers and particles volume fractions using a commercial CFD package of Ansys-Fluent. At first, the effective thermo-physical properties are used for a single-phase model CFD simulation. In this simulation, the mixture of nanoparticles suspended in a base fluid are considered as a homogeneous fluid. Comparison between the simulations and the experimental results from literature shows a significant error in the prediction of Nusselt numbers for wide range of Re numbers and nano-particle fractions in the single-phase model. With the use of a two-phase CFD model available in the Ansys-Fluent, where the interphase interactions between the particles and base fluid are considered, the model is again not able to predict the actual Nusselt number. This can be due to the inaccurate mathematical models incorporated in the software and value of the effective solid particles conductivity. To improve the Nusselt prediction, a mathematical model from literature to calculate the heat transfer between particles and the base fluid has been incorporated to Ansys–Fluent using UDF file and the effective particle conductivities have been calculated using a trial and error method. Then, correlations have been developed to relate particle conductivities versus Re numbers.

Accordingly the following results can be concluded:

- CFD prediction of Nusselt number based on single-phase approach shows a significant error relative to the experimental correlation.
- CFD prediction of Nusselt number based on Two-phase approach shows a significant error relative to the experimental correlation.
- Correlations for correct effective particle conductivity are developed based on two-phase approach.

- The correlations of effective nanoparticles conductivity show the sensitivity to Reynolds number and nanoparticles volume fraction.
- CFD prediction of Nusselt number based on Two-phase approach shows precise values by using correct particle conductivity.

# 6 Recommendations and Future Works

Based on this study, there are some recommendations for future work as follows:

1. The use of the two-phase model of Eulerian-Lagrangian model or mixture model.
2. Investigate a general dimensionless particle conductivity correlation as a function of particle volume concentration and Reynolds number.
3. Analyze the pipe under other conditions such as natural convection or mixed convection.

## Reference


1. Choi, S.U. and J. Eastman, *Enhancing thermal conductivity of fluids with nanoparticles*, 1995, Argonne National Lab., IL (United States).
2. Abu-Nada, E., Z. Masoud, and A. Hijazi, *Natural convection heat transfer enhancement in horizontal concentric annuli using nanofluids.* International Communications in Heat and Mass Transfer, 2008. **35**(5): p. 657-665.
3. Xuan, Y. and W. Roetzel, *Conceptions for heat transfer correlation of nanofluids.* International Journal of Heat and Mass Transfer, 2000. **43**(19): p. 3701-3707.
4. Roy, G., C.T. Nguyen, and P.-R. Lajoie, *Numerical investigation of laminar flow and heat transfer in a radial flow cooling system with the use of nanofluids.* Superlattices and Microstructures, 2004. **35**(3): p. 497-511.
5. Li, Q., Y. Xuan, and J. Wang, *Investigation on convective heat transfer and flow features of nanofluids.* Journal of Heat transfer, 2003. **125**: p. 151-155.
6. Mansoori, Z., et al., *Thermo-mechanical modeling of turbulent heat transfer in gas–solid flows including particle collisions.* International journal of heat and fluid flow, 2002. **23**(6): p. 792-806.
7. Liu, K., U. Choi, and K. Kasza, *Measurements of pressure drop and heat transfer in turbulent pipe flows of particulate slurries*, 1988, Argonne National Lab., IL (USA).
8. Maxwell, J.C., *A treatise on electricity and magnetism*. Vol. 1. 1881: Clarendon press.
9. Hamilton, R. and O. Crosser, *Thermal conductivity of heterogeneous two-component systems.* Industrial & Engineering chemistry fundamentals, 1962. **1**(3): p. 187-191.
10. Xuan, Y. and Q. Li, *Heat transfer enhancement of nanofluids.* International Journal of Heat and Fluid Flow, 2000. **21**(1): p. 58-64.
11. Wang, X., X. Xu, and S.U. S. Choi, *Thermal conductivity of nanoparticle-fluid mixture.* Journal of thermophysics and heat transfer, 1999. **13**(4): p. 474-480.
12. Keblinski, P., et al., *Mechanisms of heat flow in suspensions of nano-sized particles (nanofluids).* International journal of heat and mass transfer, 2002. **45**(4): p. 855-863.
13. Yu, W. and S. Choi, *The role of interfacial layers in the enhanced thermal conductivity of nanofluids: a renovated Maxwell model.* Journal of Nanoparticle Research, 2003. **5**(1-2): p. 167-171.
14. Eastman, J.A., et al., *Thermal transport in nanofluids 1.* Annu. Rev. Mater. Res., 2004. **34**: p. 219-246.
15. Jang, S.P. and S.U. Choi, *Role of Brownian motion in the enhanced thermal conductivity of nanofluids.* Applied physics letters, 2004. **84**(21): p. 4316-4318.
16. Xue, Q.-Z., *Model for effective thermal conductivity of nanofluids.* Physics letters A, 2003. **307**(5): p. 313-317.
17. Koo, J. and C. Kleinstreuer, *A new thermal conductivity model for nanofluids.* Journal of Nanoparticle Research, 2004. **6**(6): p. 577-588.
18. Leong, K., C. Yang, and S. Murshed, *A model for the thermal conductivity of nanofluids–the effect of interfacial layer.* Journal of Nanoparticle Research, 2006. **8**(2): p. 245-254.
19. Das, S.K., et al., *Nanofluids: science and technology*2008: Wiley-Interscience Hoboken, NJ.
20. Yu, W. and S. Choi, *The role of interfacial layers in the enhanced thermal conductivity of nanofluids: a renovated Hamilton–Crosser model.* Journal of Nanoparticle Research, 2004. **6**(4): p. 355-361.

21. Prasher, R., P.E. Phelan, and P. Bhattacharya, *Effect of aggregation kinetics on the thermal conductivity of nanoscale colloidal solutions (nanofluid).* Nano Letters, 2006. **6**(7): p. 1529-1534.
22. He, Y., et al., *Heat transfer and flow behaviour of aqueous suspensions of TiO< sub> 2</sub> nanoparticles (nanofluids) flowing upward through a vertical pipe.* International Journal of Heat and Mass Transfer, 2007. **50**(11): p. 2272-2281.
23. Evans, W., et al., *Effect of aggregation and interfacial thermal resistance on thermal conductivity of nanocomposites and colloidal nanofluids.* International Journal of Heat and Mass Transfer, 2008. **51**(5): p. 1431-1438.
24. Hui, P.M., et al., *Thermal conductivity of graded composites: Numerical simulations and an effective medium approximation.* Journal of materials science, 1999. **34**(22): p. 5497-5503.
25. Nan, C.-W., et al., *Effective thermal conductivity of particulate composites with interfacial thermal resistance.* Journal of Applied Physics, 1997. **81**(10): p. 6692-6699.
26. Wang, B.-X., L.-P. Zhou, and X.-F. Peng, *A fractal model for predicting the effective thermal conductivity of liquid with suspension of nanoparticles.* International Journal of Heat and Mass Transfer, 2003. **46**(14): p. 2665-2672.
27. Li, C.H., et al., *Transient and steady-state experimental comparison study of effective thermal conductivity of Al2O3/water nanofluids.* Journal of heat transfer, 2008. **130**(4): p. 040301.1-044503.4.
28. Palm, S.J., G. Roy, and C.T. Nguyen, *Heat transfer enhancement with the use of nanofluids in radial flow cooling systems considering temperature-dependent properties.* Applied Thermal Engineering, 2006. **26**(17): p. 2209-2218.
29. Putra, N., W. Roetzel, and S.K. Das, *Natural convection of nano-fluids.* Heat and Mass Transfer, 2003. **39**(8-9): p. 775-784.
30. Namburu, P.K., et al., *Numerical study of turbulent flow and heat transfer characteristics of nanofluids considering variable properties.* International journal of thermal sciences, 2009. **48**(2): p. 290-302.
31. Ding, Y., et al., *Heat transfer of aqueous suspensions of carbon nanotubes (CNT nanofluids).* International Journal of Heat and Mass Transfer, 2006. **49**(1): p. 240-250.
32. Namburu, P., et al., *Experimental investigation of viscosity and specific heat of silicon dioxide nanofluids.* Micro & Nano Letters, IET, 2007. **2**(3): p. 67-71.
33. Das, S.K., N. Putra, and W. Roetzel, *Pool boiling characteristics of nano-fluids.* International Journal of Heat and Mass Transfer, 2003. **46**(5): p. 851-862.
34. Kulkarni, D.P., D.K. Das, and G.A. Chukwu, *Temperature dependent rheological property of copper oxide nanoparticles suspension (nanofluid).* Journal of nanoscience and nanotechnology, 2006. **6**(4): p. 1150-1154.
35. Turgut, A., et al., *Thermal conductivity and viscosity measurements of water-based TiO2 nanofluids.* International Journal of Thermophysics, 2009. **30**(4): p. 1213-1226.
36. Tavman, I., et al., *Experimental investigation of viscosity and thermal conductivity of suspensions containing nanosized ceramic particles.* Archives of Materials Science, 2008. **100**: p. 100.
37. Mooney, M., *The viscosity of a concentrated suspension of spherical particles.* Journal of Colloid Science, 1951. **6**(2): p. 162-170.
38. Einstein, A., *Investigations on the Theory of the Brownian Movement*1956: Courier Dover Publications.
39. Brinkman, H., *The viscosity of concentrated suspensions and solutions.* The Journal of Chemical Physics, 1952. **20**: p. 571.

40. Pak, B.C. and Y.I. Cho, *Hydrodynamic and heat transfer study of dispersed fluids with submicron metallic oxide particles.* EXPERIMENTAL HEAT TRANSFER An International Journal, 1998. **11**(2): p. 151-170.
41. Chen, H., Y. Ding, and C. Tan, *Rheological behaviour of nanofluids.* New Journal of Physics, 2007. **9**(10): p. 367.
42. Zhu, D. and X. Wang, *Experimental investigation on viscosity of Cu-H2O nanofluids.* Journal of Wuhan University of Technology-Mater. Sci. Ed., 2009. **24**(1): p. 48-52.
43. Masoumi, N., N. Sohrabi, and A. Behzadmehr, *A new model for calculating the effective viscosity of nanofluids.* Journal of Physics D: Applied Physics, 2009. **42**(5): p. 055501.
44. Anoop, K., T. Sundararajan, and S.K. Das, *Effect of particle size on the convective heat transfer in nanofluid in the developing region.* International Journal of Heat and Mass Transfer, 2009. **52**(9): p. 2189-2195.
45. Anoop, K., et al., *Rheological and flow characteristics of nanofluids: Influence of electroviscous effects and particle agglomeration.* Journal of Applied Physics, 2009. **106**(3): p. 034909-034909-7.
46. Wen, D. and Y. Ding, *Experimental investigation into convective heat transfer of nanofluids at the entrance region under laminar flow conditions.* International Journal of Heat and Mass Transfer, 2004. **47**(24): p. 5181-5188.
47. Zeinali Heris, S., S.G. Etemad, and M. Nasr Esfahany, *Experimental investigation of oxide nanofluids laminar flow convective heat transfer.* International Communications in Heat and Mass Transfer, 2006. **33**(4): p. 529-535.
48. Li, Q. and Y. Xuan, *Convective heat transfer and flow characteristics of Cu-water nanofluid.* Science in China Series E: Technolgical Science, 2002. **45**(4): p. 408-416.
49. Yang, Y., et al., *Heat transfer properties of nanoparticle-in-fluid dispersions (nanofluids) in laminar flow.* International Journal of Heat and Mass Transfer, 2005. **48**(6): p. 1107-1116.
50. Choi, S., et al., *Anomalous thermal conductivity enhancement in nanotube suspensions.* Applied Physics Letters, 2001. **79**(14): p. 2252-2254.
51. Koo, J. and C. Kleinstreuer, *Laminar nanofluid flow in microheat-sinks.* International Journal of Heat and Mass Transfer, 2005. **48**(13): p. 2652-2661.
52. Li, J. and C. Kleinstreuer, *Thermal performance of nanofluid flow in microchannels.* International Journal of Heat and Fluid Flow, 2008. **29**(4): p. 1221-1232.
53. Santra, A.K., S. Sen, and N. Chakraborty, *Study of heat transfer due to laminar flow of copper–water nanofluid through two isothermally heated parallel plates.* International Journal of Thermal Sciences, 2009. **48**(2): p. 391-400.
54. Maïga, S.E.B., et al., *Heat transfer behaviours of nanofluids in a uniformly heated tube.* Superlattices and Microstructures, 2004. **35**(3): p. 543-557.
55. Behzadmehr, A., M. Saffar-Avval, and N. Galanis, *Prediction of turbulent forced convection of a nanofluid in a tube with uniform heat flux using a two phase approach.* International Journal of Heat and Fluid Flow, 2007. **28**(2): p. 211-219.
56. Mirmasoumi, S. and A. Behzadmehr, *Numerical study of laminar mixed convection of a nanofluid in a horizontal tube using two-phase mixture model.* Applied Thermal Engineering, 2008. **28**(7): p. 717-727.
57. Mirmasoumi, S. and A. Behzadmehr, *Effect of nanoparticles mean diameter on mixed convection heat transfer of a nanofluid in a horizontal tube.* International Journal of Heat and Fluid Flow, 2008. **29**(2): p. 557-566.

58. Akbarinia, A. and R. Laur, *Investigating the diameter of solid particles effects on a laminar nanofluid flow in a curved tube using a two phase approach.* International Journal of Heat and Fluid Flow, 2009. **30**(4): p. 706-714.
59. Bianco, V., et al., *Numerical investigation of nanofluids forced convection in circular tubes.* Applied Thermal Engineering, 2009. **29**(17): p. 3632-3642.
60. Kurowski, L., K. Chmiel-Kurowska, and J. Thulliea, *Numerical simulation of heat transfer in nanofluids.* Computer Aided Chemical Engineering, 2009. **26**: p. 967-972.
61. Haghshenas Fard, M., M.N. Esfahany, and M. Talaie, *Numerical study of convective heat transfer of nanofluids in a circular tube two-phase model versus single-phase model.* International Communications in Heat and Mass Transfer, 2010. **37**(1): p. 91-97.
62. Lotfi, R., Y. Saboohi, and A. Rashidi, *Numerical study of forced convective heat transfer of nanofluids: comparison of different approaches.* International Communications in Heat and Mass Transfer, 2010. **37**(1): p. 74-78.
63. Fluent, A., *Ansys Fluent 12.0 user guide.* ANSYS Inc, 2009.
64. Launder, B.E. and D. Spalding, *The numerical computation of turbulent flows.* Computer methods in applied mechanics and engineering, 1974. **3**(2): p. 269-289.
65. Kalteh, M., et al., *Eulerian–Eulerian two-phase numerical simulation of nanofluid laminar forced convection in a microchannel.* International Journal of Heat and Fluid Flow, 2011. **32**(1): p. 107-116.
66. Whitaker, S., *Forced convection heat transfer correlations for flow in pipes, past flat plates, single cylinders, single spheres, and for flow in packed beds and tube bundles.* AIChE Journal, 1972. **18**(2): p. 361-371.
67. Kuipers, J., W. Prins, and W. Van Swaaij, *Numerical calculation of wall-to-bed heat-transfer coefficients in gas-fluidized beds.* AIChE Journal, 1992. **38**(7): p. 1079-1091.
68. Bergman, T.L., et al., *Fundamentals of heat and mass transfer*2011: John Wiley & Sons.

## Appendix A

### Single-Phase Model

Since accuracy of effective single phase is investigated in this study, the single phase mathematical models are first introduced. By solving three governing equations, continuity, conservation of momentum and conservation of mass, one can find the temperature contour throughout the flow. Once the temperature distribution found, the Nusselt number can be calculated.

Since in turbulent regime the flow properties fluctuate instantly, the time-averaged Reynolds approach is used for governing equations as below.

1. Continuity Equation (Time-averaged equation of continuity)

   The continuity equation can be written in each instant as follow:

$$\frac{\partial(\rho_{eff}(t))}{\partial t} + \nabla.((\rho_{eff}(t))(V(t)) = S_{mass} \qquad \textbf{0-1}$$

$S_m$ represents a source of mass according mass production or destruction (i.e. vaporization or fluidization) which is equal zero in this study.

Substituting

$$\rho_{eff} = \bar{\rho}_{eff} + \rho'_{eff}, \quad V(t) = \bar{V} + V' \qquad \textbf{0-2}$$

and time averaging:

$$\overline{\frac{\partial(\bar{\rho}_{eff} + \rho'_{eff})}{\partial t} + \nabla.((\bar{\rho}_{eff} + \rho'_{eff})(\bar{V} + V'))} = 0$$
$$\rightarrow \frac{\partial(\overline{\rho_{eff}} + \overline{\rho'_{eff}})}{\partial t} + \nabla.((\overline{\bar{\rho}_{eff}\bar{V}} + \overline{\rho'_{eff}\bar{V}} + \overline{V'\bar{\rho}_{eff}} + \overline{\rho'_{eff}V'}) = 0 \qquad \textbf{0-3}$$

This differential equation can be simplified since

$$\overline{\rho'_{eff}} = 0$$
*and*
$$\overline{V_{eff}'} = 0$$

**0-4**

Hence for incompressible flow the continuity equation can be determined as:

$$\nabla.\bar{V} = 0 \qquad \textbf{0-5}$$

For cylindrical coordinate system and by underestimation the changes in tangential direction one can write:

$$\frac{\partial(\bar{v}_z)}{\partial z} + \frac{1}{r}\frac{\partial(r\overline{v_r})}{\partial r} = 0 \qquad \textbf{0-6}$$

2. Conservation of momentum

   The momentum equation of incompressible and Newtonian turbulent flow in each time can be as follow:

$$\rho_{eff}((\frac{\partial(V)}{\partial t}) + (V).\nabla(V)) = F_B - \nabla P + \mu_{eff}\nabla^2(V) + S_{Moentum} \qquad \textbf{0-7}$$

By substituting the measures of $V = \bar{V} + V'$, $P = \bar{P} + P'$ in the momentum equation and averaging the whole of equation rather to time one can write:

$$\overline{\rho_{eff}((\frac{\partial(\bar{V}+V')}{\partial t}) + (\bar{V}+V').\nabla(\bar{V}+V'))} = F_B - \nabla\overline{(\bar{P}+P')} + \overline{\mu_{eff}\nabla^2(\bar{V}+V')} + S_{Moentum}$$

**0-8**

Since the value of momentum source and average of fluctuating parameters are equal zero the Equation 8 can be simplified as:

$$\rho_{eff}(\frac{\partial\bar{V}}{\partial t} + \bar{V}.\nabla\bar{V} + \overline{V'.\nabla V'}) = F_B - \nabla\bar{P} + \mu_{eff}\nabla^2\bar{V}$$

**0-9**

According the continuity equation:

$$\nabla.V = 0 \qquad \textbf{0-10}$$

That implies:

$$\nabla.(\bar{V}+V') = \nabla.\bar{V} + \nabla.V' = 0 \qquad \textbf{0-11}$$

Based on Equation 5 one can write:

$$\nabla.V' = 0 \qquad \textbf{0-12}$$

So the Equation 11 can be written as:

$$\rho_{eff}(\frac{\partial \bar{V}}{\partial t} + \bar{V}.\nabla\bar{V} + \overline{\nabla.V'V'}) = F_B - \nabla\bar{P} + \mu_{eff}\nabla^2\bar{V} \qquad \textbf{0-13}$$

$$\rho_{eff}(\frac{\partial \bar{V}}{\partial t} + \bar{V}.\nabla\bar{V}) = F_B - \nabla\bar{P} + \mu_{eff}\nabla^2\bar{V} - \rho_{eff}\overline{\nabla.V'V'} \qquad \textbf{0-14}$$

Where the two last parameters in the left hand side are known as shear and Reynolds (turbulence) stress respectively and can be calculated as follows:

$$(-\overline{\rho_{eff}V'V'})_{ij} = -\overline{\rho_{eff}v_i'v_j'} \qquad \textbf{0-15}$$

$$\bar{\tau}_{ij} = \mu_{eff}(\frac{\partial \bar{v}_i}{\partial x_j} + \frac{\partial \bar{v}_j}{\partial x_i}) \qquad \textbf{0-16}$$

$$\overline{\tau^T}_{ij} = -\overline{\rho_{eff}v_i'v_j'} \qquad \textbf{0-17}$$

$$\overline{\tau_{ij_{Tot}}} = \overline{\tau_{ij}} + \overline{\tau_{ij}^T} = \mu_{eff}(\frac{\partial \bar{v}_i}{\partial x_j} + \frac{\partial \bar{v}_j}{\partial x_i}) - \overline{\rho_{eff}v_i'v_j'} \qquad \textbf{0-18}$$

$$\rho_{eff}(\frac{\partial \bar{V}}{\partial t} + \bar{V}.\nabla\bar{V}) = F_B - \nabla\bar{P}\delta_{ij} + \nabla.\overline{\tau_{ij_{Tot}}} \qquad \textbf{0-19}$$

Due to constant wall-heat flux boundary condition and also fully developed turbulent flow, if the changes in tangential direction are ignored the steady state axisymmetric governing equations can be considered in this case.

$$\rho_{eff}[\frac{\partial(\overline{v_z v_z})}{\partial z} + \frac{1}{r}\frac{\partial(r\overline{v_r v_z})}{\partial r} = F_{B_z} - \frac{\partial \bar{P}}{\partial z} + \frac{\partial \overline{\tau_{zz}}}{\partial z} + \frac{1}{r}\frac{\partial(r\overline{\tau_{zr}})}{\partial r} + \frac{\partial \overline{\tau_{zz}^T}}{\partial z} + \frac{\partial \overline{\tau_{zr}^T}}{\partial r}$$

**0-20**

$$\rho_{eff}[\frac{\partial(\overline{v_z v_r})}{\partial z}+\frac{1}{r}\frac{\partial(r\overline{v_r v_r})}{\partial r}=F_{B_r}-\frac{\partial \overline{P}}{\partial r}+\frac{\partial \overline{\tau_{rz}}}{\partial z}+\frac{1}{r}\frac{\partial(r\overline{\tau_{rr}})}{\partial r}+\frac{\overline{\tau}_{\theta\theta}}{r}+\frac{\partial \overline{\tau_{rz}}^{T}}{\partial z}+\frac{\partial \overline{\tau_{rr}}^{T}}{\partial r}$$ **0-21**

Where the tension tensor components can be introduced as:

$$\overline{\tau_{zz}}=2\mu_{eff}\frac{\partial \overline{v_z}}{\partial z}$$ **0-22**

$$\overline{\tau_{rr}}=2\mu_{eff}\frac{\partial \overline{v_r}}{\partial r}$$ **0-23**

$$\overline{\tau_{\theta\theta}}=-2\mu_{eff}\frac{\overline{v_r}}{r}$$ **0-24**

$$\overline{\tau_{rz}}=\overline{\tau_{zr}}=\mu_{eff}(\frac{\partial \overline{v_z}}{\partial r}+\frac{\partial \overline{v_r}}{\partial z})$$ **0-25**

And also the turbulent tension can be defined as:

$$\overline{\tau_{zr}^{T}}=\overline{\tau_{rz}^{T}}=-\rho_{eff}\overline{v_z' v_r'}$$ **0-26**

$$\overline{\tau_{rr}^{T}}=-\rho_{eff}\overline{v_r'^{2}}$$ **0-27**

$$\overline{\tau_{zz}^{T}}=-\rho_{eff}\overline{v_z'^{2}}$$ **0-28**

3. The standard K-Ɛ model

Due to the appearance of turbulent stress parameter two kinds of transport equations are needed. The first one is called turbulent kinetic energy transportation equation as:

$$\frac{\partial(\rho_{eff}k)}{\partial t}+div(\rho_{eff}kV)=div[\frac{\mu_t}{\sigma_k}grad(k)]+2\mu_t S_{ij}.S_{ij}-\rho_{eff}\varepsilon$$ **0-29**

And another one is the rate of dissipation transportation equation.

$$\frac{\partial(\rho_{eff}\varepsilon)}{\partial t}+div(\rho_{eff}\varepsilon V)=div[\frac{\mu_t}{\sigma_\varepsilon}grad(\varepsilon)]+C_{1\varepsilon}\frac{\varepsilon}{k}2\mu_t S_{ij}.S_{ij}-C_{2\varepsilon}\rho_{eff}\frac{\varepsilon^2}{k}$$ **0-30**

Where k and Ɛ are defined as:

$$k=\frac{1}{2}(\overline{v_z'^{2}}+\overline{v_r'^{2}})$$ **0-31**

$$\varepsilon = 2\upsilon_{eff}\overline{s_{ij}^{'}.s_{ij}^{'}} \quad \textbf{0-32}$$

And also the S and $\mu_t$ called rate of deformation and turbulent viscosity respectively are calculated as follows:

$$S_{ij} = \begin{pmatrix} S_{zz} & S_{zr} & S_{z\theta} \\ S_{rz} & S_{rr} & S_{r\theta} \\ S_{\theta z} & S_{\theta r} & S_{\theta\theta} \end{pmatrix} \quad \textbf{0-33}$$

$$S_{zz}(t) = \overline{S_{zz}} + s_{zz}^{'} = \frac{\partial \overline{v_z}}{\partial z} + \frac{\partial v_z^{'}}{\partial z} \quad \textbf{0-34}$$

$$S_{rr}(t) = \overline{S_{rr}} + s_{rr}^{'} = \frac{\partial \overline{v_r}}{\partial r} + \frac{\partial v_r^{'}}{\partial r} \quad \textbf{0-35}$$

$$S_{\theta\theta}(t) = \overline{S_{\theta\theta}} + s_{\theta\theta}^{'} = \frac{\partial \overline{v_\theta}}{\partial z} + \frac{\partial v_\theta^{'}}{\partial z} = 0 \quad \textbf{0-36}$$

$$S_{zr} = S_{rz} = \overline{S_{rz}} + s_{rz}^{'} = \frac{1}{2}[\frac{\partial \overline{v_z}}{\partial r} + \frac{\partial \overline{v_r}}{\partial z}] + \frac{1}{2}[\frac{\partial v_z^{'}}{\partial r} + \frac{\partial v_r^{'}}{\partial z}] \quad \textbf{0-37}$$

$$S_{z\theta} = S_{\theta z} = \overline{S_{\theta z}} + s_{\theta z}^{'} = 0 \quad \textbf{0-38}$$

$$S_{r\theta} = S_{\theta r} = \overline{S_{\theta r}} + s_{\theta r}^{'} = 0 \quad \textbf{0-39}$$

$$\mu_t = \rho_{eff} C_\mu \frac{k^2}{\varepsilon} \quad \textbf{0-40}$$

$$C_\mu = 0.09, \sigma_k = 1.00, \sigma_\varepsilon = 1.30, C_{1\varepsilon} = 1.44, C_{2\varepsilon} = 1.92$$

4. Conservation of energy

The temperature distribution can be found by solving the energy equation. According the general form of transport equation for scalar properties the energy equation can be resulted as:

$$\rho_{eff} c_{p,eff} \frac{\partial \overline{T}}{\partial t} + div(\rho_{eff} c_{p,eff} \overline{T}\overline{V}) = div(k_{eff}\, grad(\overline{T})) - \rho_{eff} c_{p,eff} [\frac{\partial \overline{(v_z^{'}T^{'})}}{\partial z} + \frac{\partial \overline{(v_r^{'}T^{'})}}{\partial r}] \quad \textbf{0-41}$$
$$+\Phi + S_{energy}$$

where the Φ and S are known as viscous dissipation and energy source respectively. According the case of study that is without internal energy and by neglecting the energy produced by viscous dissipation the Equation 41 can be derived as:

$$\overline{v_z}\frac{\partial \overline{T}}{\partial z}+\overline{v_r}\frac{\partial \overline{T}}{\partial r}=\frac{k_{eff}}{\rho_{eff}c_{p,eff}}div(grad(\overline{T}))-[\frac{\partial(\overline{v_z^{'}T^{'}})}{\partial z}+\frac{\partial(\overline{v_r^{'}T^{'}})}{\partial r}] \quad \textbf{0-42}$$

**Eulerian-Eulerian Two-Phase Model**

In this chapter the governing equations are derived for Eulerian-Eulerian two-phase model. Although in this case the approach is roughly same as single phase method, each phase has its specific equation with considering interphase interactions and phase volume fraction.

The continuity equation (time-averaged equation of continuity) for each phase can be written as:

$$\frac{\partial(\varphi_l \bar{v}_{z_l})}{\partial z}+\frac{1}{r}\frac{\partial(\varphi_l r\overline{v_{r_l}})}{\partial r}=0 \quad \textbf{0-43}$$

$$\frac{\partial(\varphi_p \bar{v}_{z_p})}{\partial z}+\frac{1}{r}\frac{\partial(\varphi_p r\overline{v_{r_p}})}{\partial r}=0 \quad \textbf{0-44}$$

where

$$\varphi_l+\varphi_p=1 \quad \textbf{0-45}$$

The conservation of momentum for liquid phase can be written as:

$$\varphi_l\rho_l[\frac{\partial \overline{v}_{z_l}}{\partial t}+\frac{\partial(\overline{v_{z_l}v_{z_l}})}{\partial z}+\frac{1}{r}\frac{\partial(r\overline{v_{r_l}v_{z_l}})}{\partial r}=(F_{vm})_z+(F_d)_z-\varphi_l[\frac{\partial \overline{P}}{\partial z}-\frac{\partial \overline{\tau_{zz_l}}}{\partial z}-\frac{1}{r}\frac{\partial(r\overline{\tau_{zr_l}})}{\partial r} -\frac{\partial \overline{\tau_{zz_l}}^{T}}{\partial z}-\frac{\partial \overline{\tau_{zr_l}}^{T}}{\partial r}] \quad \textbf{0-46}$$

$$\varphi_l \rho_l [\frac{\partial \overline{v}_{r_l}}{\partial t} + \frac{\partial (\overline{v_{z_l} v_{r_l}})}{\partial z} + \frac{1}{r}\frac{\partial (r\overline{v_{r_l} v_{r_l}})}{\partial r} = (F_{vm})_r + (F_d)_r - \varphi_l [\frac{\partial \overline{P}}{\partial r} - \frac{\partial \overline{\tau_{rz_l}}}{\partial z} - \frac{1}{r}\frac{\partial (r\overline{\tau_{rr_l}})}{\partial r} - \frac{\overline{\tau}_{\theta\theta_l}}{r} - \frac{\partial \overline{\tau_{rz_l}}^{T}}{\partial z} - \frac{\partial \overline{\tau_{rr_l}}^{T}}{\partial r}]$$ **0-47**

Where the tension tensor components can be introduced as:

$$\overline{\tau_{zz_l}} = 2\mu_l \frac{\partial \overline{v_{z_l}}}{\partial z}$$ **0-48**

$$\overline{\tau_{rr_l}} = 2\mu_l \frac{\partial \overline{v_{r_l}}}{\partial r}$$ **0-49**

$$\overline{\tau_{\theta\theta_l}} = -2\mu_l \frac{\overline{v_{r_l}}}{r}$$ **0-50**

$$\overline{\tau_{rz_l}} = \overline{\tau_{zr_l}} = \mu_l (\frac{\partial \overline{v_{z_l}}}{\partial r} + \frac{\partial \overline{v_{r_l}}}{\partial z})$$ **0-51**

And also the turbulent stress can be defined as:

$$\overline{\tau_{zr_l}^{T}} = \overline{\tau_{rz_l}^{T}} = -\rho_l \overline{v'_{z_l} v'_{r_l}}$$ **0-52**

$$\overline{\tau_{rr_l}^{T}} = -\rho_l \overline{v'^{2}_{r_l}}$$ **0-53**

$$\overline{\tau_{zz_l}^{T}} = -\rho_l \overline{v'^{2}_{z_l}}$$ **0-54**

On the other hand, for particle phase one can write:

$$\varphi_p \rho_p [\frac{\partial \overline{v}_{z_p}}{\partial t} + \frac{\partial (\overline{v_{z_p} v_{z_p}})}{\partial z} + \frac{1}{r}\frac{\partial (r\overline{v_{r_p} v_{z_p}})}{\partial r} = (F_{col})_z - (F_{vm})_z - (F_d)_z - \varphi_p [\frac{\partial \overline{P}}{\partial z} - \frac{\partial \overline{\tau_{zz_p}}}{\partial z} - \frac{1}{r}\frac{\partial (r\overline{\tau_{zr_p}})}{\partial r} - \frac{\partial \overline{\tau_{zz_p}}^{T}}{\partial z} - \frac{\partial \overline{\tau_{zr_p}}^{T}}{\partial r}]$$ **0-55**

$$\varphi_p \rho_p [\frac{\partial \overline{v}_{r_p}}{\partial t} + \frac{\partial (\overline{v_{z_p} v_{r_p}})}{\partial z} + \frac{1}{r}\frac{\partial (r\overline{v_{r_p} v_{r_p}})}{\partial r} = (F_{col})_r - (F_{vm})_r - (F_d)_r - \varphi_p [\frac{\partial \overline{P}}{\partial r} - \frac{\partial \overline{\tau_{rz_p}}}{\partial z} - \frac{1}{r}\frac{\partial (r\overline{\tau_{rr_p}})}{\partial r} - \frac{\overline{\tau}_{\theta\theta_p}}{r} - \frac{\partial \overline{\tau_{rz_p}}^{T}}{\partial z} - \frac{\partial \overline{\tau_{rr_p}}^{T}}{\partial r}]$$ **0-56**

Where the tension tensor components can be introduced as:

$$\overline{\tau_{zz_p}} = 2\mu_p \frac{\partial \overline{v_{z_p}}}{\partial z} \quad \textbf{0-57}$$

$$\overline{\tau_{rr_p}} = 2\mu_p \frac{\partial \overline{v_{r_p}}}{\partial r} \quad \textbf{0-58}$$

$$\overline{\tau_{\theta\theta_p}} = -2\mu_p \frac{\overline{v_{r_p}}}{r} \quad \textbf{0-59}$$

$$\overline{\tau_{rz_p}} = \overline{\tau_{zr_p}} = \mu_p \left(\frac{\partial \overline{v_{z_p}}}{\partial r} + \frac{\partial \overline{v_{r_p}}}{\partial z}\right) \quad \textbf{0-60}$$

And also the turbulent stress can be defined as:

$$\overline{\tau_{zr_p}^{\,T}} = \overline{\tau_{rz_p}^{\,T}} = -\rho_p \overline{v'_{z_p} v'_{r_p}} \quad \textbf{0-61}$$

$$\overline{\tau_{rr_p}^{\,T}} = -\rho_p \overline{v'^{2}_{r_p}} \quad \textbf{0-62}$$

$$\overline{\tau_{zz_p}^{\,T}} = -\rho_p \overline{v'^{\,2}_{z_p}} \quad \textbf{0-63}$$

$F_{col}$, $F_{vm}$ and $F_d$ are defined as collision, virtual mass and drag interphase forces respectively. According the dilute mixture of nanofluid the collision and virtual mass forces can be neglected in this study. By considering interphase drag force the correlation offered by Schiller-Naumann [65] used due to the literatures as below:

$$F_d = \beta(\vec{V}_l - \vec{V}_p) \quad \textbf{0-64}$$

$$\beta = \frac{3}{4}\frac{C_D}{d_p}\varphi_p \rho_l \left|V_l - V_p\right| \quad \textbf{0-65}$$

$$C_D = \frac{24}{\mathrm{Re}_p}(1 + 0.15\,\mathrm{Re}_p^{\,0.687}) \quad \textbf{0-66}$$

$$\mathrm{Re}_p = \frac{\varphi_l \rho_l \left|\vec{V}_l - \vec{V}_p\right| d_p}{\mu_l} \quad \textbf{0-67}$$

The standard K-Ɛ model for each phase can be derived as:

(Liquid Phase)

$$\frac{\partial(\varphi_l \rho_l k_l)}{\partial t} + div(\varphi_l \rho_l k_l V_l) = div[\frac{\varphi_l \mu_{t_l}}{\sigma_k} grad(k_l)] + 2\varphi_l \mu_{t_l} S_{ij_l}.S_{ij_l} - \varphi_l \rho_l \varepsilon_l \quad \textbf{0-68}$$

$$\frac{\partial(\varphi_l \rho_l \varepsilon_l)}{\partial t} + div(\varphi_l \rho_l \varepsilon_l V_l) = div[\frac{\varphi_l \mu_{t_l}}{\sigma_\varepsilon} grad(\varepsilon_l)] + \varphi_l C_{1\varepsilon} \frac{\varepsilon_l}{k_l} 2\mu_{t_l} S_{ij_l}.S_{ij_l} - \varphi_l C_{2\varepsilon} \rho_l \frac{{\varepsilon_l}^2}{k_l} \quad \textbf{0-69}$$

Where the turbulent kinetic energy is defined for liquid:

$$k_l = \frac{1}{2}(\overline{{v'_{z_l}}^2} + \overline{{v'_{r_l}}^2}) \quad \textbf{0-70}$$

And also the deformation tensor and its components can be introduced:

$$S_{ij_l} = \begin{pmatrix} S_{zz_l} & S_{zr_l} & S_{z\theta_l} \\ S_{rz_l} & S_{rr_l} & S_{r\theta_l} \\ S_{\theta z_l} & S_{\theta r_l} & S_{\theta\theta_l} \end{pmatrix} \quad \textbf{0-71}$$

$$S_{zz_l}(t) = \overline{S_{zz_l}} + s'_{zz_l} = \frac{\partial \overline{v_{z_l}}}{\partial z} + \frac{\partial v'_{z_l}}{\partial z} \quad \textbf{0-72}$$

$$S_{rr_l}(t) = \overline{S_{rr_l}} + s'_{rr_l} = \frac{\partial \overline{v_{r_l}}}{\partial r} + \frac{\partial v'_{r_l}}{\partial r} \quad \textbf{0-73}$$

$$S_{\theta\theta_l}(t) = \overline{S_{\theta\theta_l}} + s'_{\theta\theta_l} = \frac{\partial \overline{v_{\theta_l}}}{\partial z} + \frac{\partial v'_{\theta_l}}{\partial z} = 0 \quad \textbf{0-74}$$

$$S_{zr_l} = S_{rz_l} = \overline{S_{rz_l}} + s'_{rz_l} = \frac{1}{2}[\frac{\partial \overline{v_{z_l}}}{\partial r} + \frac{\partial \overline{v_{r_l}}}{\partial z}] + \frac{1}{2}[\frac{\partial v'_{z_l}}{\partial r} + \frac{\partial v'_{r_l}}{\partial z}] \quad \textbf{0-75}$$

$$S_{z\theta_l} = S_{\theta z_l} = \overline{S_{\theta z_l}} + s'_{\theta z_l} = 0 \quad \textbf{0-76}$$

$$S_{r\theta_l} = S_{\theta r_l} = \overline{S_{\theta r_l}} + s'_{\theta r_l} = 0 \quad \textbf{0-77}$$

$$\varepsilon_l = 2\upsilon_l \overline{s'_{ij_l}.s'_{ij_l}} \quad \textbf{0-78}$$

$$\mu_{t_l} = \rho_l C_\mu \frac{{k_l}^2}{\varepsilon_l} \quad \textbf{0-79}$$

$$C_\mu = 0.09, \sigma_k = 1.00, \sigma_\varepsilon = 1.30, C_{1\varepsilon} = 1.44, C_{2\varepsilon} = 1.92$$

(Solid Particle Phase)

$$\frac{\partial(\varphi_p \rho_p k_p)}{\partial t} + div(\varphi_p \rho_p k_p V_p) = div[\frac{\varphi_p \mu_{tp}}{\sigma_k} grad(k_p)] + 2\varphi_p \mu_{t_p} S_{ij_p}.S_{ij_p} - \varphi_p \rho_p \varepsilon_p \quad \textbf{0-80}$$

$$\frac{\partial(\varphi_p\rho_p\varepsilon_p)}{\partial t}+div(\varphi_p\rho_p\varepsilon_p V_p)=div[\frac{\varphi_p\mu_{t_p}}{\sigma_\varepsilon}grad(\varepsilon_p)]+$$

$$\varphi_p C_{1\varepsilon}\frac{\varepsilon_p}{k_p}2\mu_{t_p}S_{ij_p}.S_{ij_p}-\varphi_p C_{2\varepsilon}\rho_p\frac{{\varepsilon_p}^2}{k_p} \quad \textbf{0-81}$$

Where the turbulent kinetic energy is defined for solid particles:

$$k_p=\frac{1}{2}(\overline{{v'_{z_p}}^2}+\overline{{v'_{r_p}}^2}) \quad \textbf{0-82}$$

And also the deformation tensor and its components can be introduced:

$$S_{ij_p}=\begin{pmatrix} S_{zz_p} & S_{zr_p} & S_{z\theta_p} \\ S_{rz_p} & S_{rr_p} & S_{r\theta_p} \\ S_{\theta z_p} & S_{\theta r_p} & S_{\theta\theta_p} \end{pmatrix} \quad \textbf{0-83}$$

$$S_{zz_p}(t)=\overline{S_{zz_p}}+s'_{zz_p}=\frac{\partial\overline{v_{z_p}}}{\partial z}+\frac{\partial v'_{z_p}}{\partial z} \quad \textbf{0-84}$$

$$S_{rr_p}(t)=\overline{S_{rr_p}}+s'_{rr_p}=\frac{\partial\overline{v_{r_p}}}{\partial r}+\frac{\partial v'_{r_p}}{\partial r} \quad \textbf{0-85}$$

$$S_{\theta\theta_p}(t)=\overline{S_{\theta\theta_p}}+s'_{\theta\theta_p}=\frac{\partial\overline{v_{\theta_p}}}{\partial z}+\frac{\partial v'_{\theta_p}}{\partial z}=0 \quad \textbf{0-86}$$

$$S_{zr_p}=S_{rz_p}=\overline{S_{rz_p}}+s'_{rz_p}=\frac{1}{2}[\frac{\partial\overline{v_{z_p}}}{\partial r}+\frac{\partial\overline{v_{r_p}}}{\partial z}]+\frac{1}{2}[\frac{\partial v_{z_p}{}'}{\partial r}+\frac{\partial v_{r_p}{}'}{\partial z}] \quad \textbf{0-87}$$

$$S_{z\theta_p}=S_{\theta z_p}=\overline{S_{\theta z_p}}+s'_{\theta z_p}=0 \quad \textbf{0-88}$$

$$S_{r\theta_p}=S_{\theta r_p}=\overline{S_{\theta r_p}}+s'_{\theta r_p}=0 \quad \textbf{0-89}$$

$$\varepsilon_p=2\upsilon_p\overline{s'_{ij_p}.s'_{ij_p}} \quad \textbf{0-90}$$

$$\mu_{t_p}=\rho_p C_\mu\frac{{k_p}^2}{\varepsilon_p} \quad \textbf{0-91}$$

$$C_\mu=0.09,\sigma_k=1.00,\sigma_\varepsilon=1.30,C_{1\varepsilon}=1.44,C_{2\varepsilon}=1.92$$

The conservation of energy for each phase and direction can be derived:

$$\varphi_l \rho_l c_{p,l} \frac{\partial \overline{T_l}}{\partial t} + div(\varphi_l \rho_l c_{p,l} \overline{T_l} \overline{V_l}) = div(\varphi_l k_{eff,l} grad(\overline{T_l}))$$
$$-\varphi_l \rho_l c_{p,l} [+ \frac{\partial \overline{(v_{z_l}^{'} T_l^{'})}}{\partial z} + \frac{\partial \overline{(v_{r_l}^{'} T_l^{'})}}{\partial r}] - h_v (T_l - T_p) + \Phi + S_{energy} \quad \textbf{0-92}$$

$$\varphi_l (\overline{v_{z_l}} \frac{\partial \overline{T_l}}{\partial z} + \overline{v_{r_l}} \frac{\partial \overline{T_l}}{\partial r}) = \frac{k_{eff,l}}{\rho_l c_{p,l}} div(\varphi_l grad(\overline{T_l}))$$
$$-\varphi_l [\frac{\partial \overline{(v_{z_l}^{'} T_l^{'})}}{\partial z} + \frac{\partial \overline{(v_{r_l}^{'} T_l^{'})}}{\partial r}] - h_v (T_l - T_p) \quad \textbf{0-93}$$

$$\varphi_p \rho_p c_{p,p} \frac{\partial \overline{T_p}}{\partial t} + div(\varphi_p \rho_p c_{p,p} \overline{T_p} \overline{V_p}) = div(\varphi_p k_{eff,p} grad(\overline{T_p}))$$
$$-\varphi_p \rho_p c_{p,p} [\frac{\partial \overline{(v_{z_p}^{'} T_p^{'})}}{\partial z} + \frac{\partial \overline{(v_{r_p}^{'} T_p^{'})}}{\partial r}] + h_v (T_l - T_p) + \Phi + S_{energy} \quad \textbf{0-94}$$

$$\varphi_p (\overline{v_{z_p}} \frac{\partial \overline{T_p}}{\partial z} + \overline{v_{r_p}} \frac{\partial \overline{T_p}}{\partial r}) = \frac{k_{eff,p}}{\rho_p c_{p,p}} div(\varphi_p grad(\overline{T_p}))$$
$$-\varphi_p [\frac{\partial \overline{(v_{z_p}^{'} T_p^{'})}}{\partial z} + \frac{\partial \overline{(v_{r_p}^{'} T_p^{'})}}{\partial r}] + h_v (T_l - T_p) \quad \textbf{0-95}$$

## Appendix B

### Turbulent Nusselt Number Correlations

The Dittus-Boelter correlation for calculating Nusselt number is written as below [68]:

$$Nu = 0.023 \mathrm{Re}^{4/5} \mathrm{Pr}^{0.4}$$
$$0.7 \le \mathrm{Pr} \le 120,$$
$$2500 \le \mathrm{Re} \le 1.24 \times 10^5,$$
$$L / D > 60 \quad \textbf{0-1}$$

where L and D are the length and diameter of the tube, respectively, and the characteristic dimension in the Nusselt and Reynolds numbers is the tube diameter D. The equation can

be used for small to moderate temperature differences between the tube wall and the fluid at inlet, Tw_ Ti, with all the physical properties evaluated at the bulk temperature Tm.

On the other hand, other correlation recommended by Gnielinski can be considered [68]:

$$Nu = \frac{(f/8)(\mathrm{Re}_D - 10^3)\,\mathrm{Pr}}{1 + 12.7(f/8)^{1/2}(\mathrm{Pr}^{2/3} - 1)}$$
$$0.5 \le \mathrm{Pr} \le 20000,$$
$$3000 \le \mathrm{Re} \le 5 \times 10^6,$$
$$(L/D) \ge 10 \qquad \textbf{0-2}$$

in which the physical properties must be evaluated at the bulk temperature Tm, while the Fanning friction factor f defined by the so-called Fanning equation can be calculated through the relation given by Filonenko for isothermal flows in smooth tubes [68]:

$$f = (0.790 \ln \mathrm{Re}_D - 1.64)^{-2} \qquad \textbf{0-3}$$

**Nanofluid Nusselt Number correlation**

Li et al.[48] correlation for nanofluid Nusselt number is recommended as below:

$$Nu_{nf} = 0.0059(1.0 + 7.6286\phi^{0.6886} Pe_d^{0.001})\,\mathrm{Re}_{nf}^{0.9238}\,\mathrm{Pr}_{nf}^{0.4} \qquad \textbf{0-4}$$

Where the particle Peclet number $\mathrm{Pe_d}$, is defined as:

$$Pe_d = \frac{u_m . d_p}{\alpha_{nf}} \qquad \textbf{0-5}$$

The Reynolds number of nanofluid $\mathrm{Re_{nf}}$ is defined as:

$$\mathrm{Re}_{nf} = \frac{u_m . D}{\upsilon_{nf}} \qquad \textbf{0-6}$$

The Prandlt number of the nanofluid $\mathrm{Pr_{nf}}$ is defined as:

$$\mathrm{Pr}_{nf} = \frac{\upsilon_{nf}}{\alpha_{nf}} \qquad \textbf{0-7}$$

To calculate this parameter, the thermal diffusivity of the nanofluid $\alpha_{nf}$ is defined as:

$$\alpha_{nf} = \frac{k_{eff}}{(\rho c_p)_{eff}} = \frac{k_{eff}}{(1-\phi)(\rho c_p)_f + \phi(\rho c_p)_s} \quad \textbf{0-8}$$